Article

Modelled Multidecadal Trends of Lightning and (Very) Large Hail in Europe and North America (1950–2021)

Francesco Battaglioli *, Pieter Groenemeijer, Tomas Pucik, Mateusz Taszarek, Uwe Ulbrich, Henning Rust

Posted Date: 3 August 2023

doi: 10.20944/preprints202308.0314.v1

Keywords: Hail; Lightning; Climate change; Regression analysis; Trends; Reanalysis data

Article

Modelled Multidecadal Trends of Lightning and (Very) Large Hail in Europe and North America (1950–2021)

Francesco Battaglioli [1,2], Pieter Groenemeijer [3,1], Tomáš Púčik [3], Mateusz Taszarek [4,5], Uwe Ulbrich [2] and Henning Rust [2]

[1] European Severe Storms Laboratory e.V. (ESSL), Wessling, Germany
[2] Institut für Meteorologie, Freie Universität Berlin, Berlin, Germany
[3] European Severe Storms Laboratory (ESSL) – Science & Training, Wiener Neustadt, Austria
[4] Department of Meteorology and Climatology, Adam Mickiewicz University, Poznań, Poland
[5] National Severe Storms Laboratory, Norman, Oklahoma, United States
* Correspondence: francesco.battaglioli@essl.org

Abstract: We have developed additive logistic models for the occurrence of lightning, large (≥ 2 cm), and very large (≥ 5 cm) hail to investigate the evolution of these hazards in the past, in the future, and for forecasting applications. The models, trained with lightning observations, hail reports, and predictors from atmospheric reanalysis, assign an hourly probability to any location and time on a 0.25° × 0.25° × 1-hourly grid as a function of reanalysis-derived predictor parameters, selected following an ingredients-based approach. The resulting hail models outperform the Significant Hail Parameter and the simulated climatological spatial distributions and annual cycles of lightning and hail are consistent with observations from storm report databases, radar, and lightning detection data. As a corollary result, CAPE released above the -10°C isotherm was found to be a more universally skilful predictor for large hail than CAPE. In the period 1950–2021, the models applied to the ERA5 reanalysis indicate significant increases of lightning and hail across most of Europe, primarily due to rising low-level moisture. The strongest modelled hail increases occur in northern Italy with increasing rapidity after 2010. Here, very large hail has become 3 times more likely than it was in the 1950s. Across North America trends are comparatively small, apart from isolated significant increases in the direct lee of the Rocky Mountains and across the Canadian Plains. In the southern Plains, a period of enhanced storm activity occurred in the 1980s and 1990s.

Keywords: hail; lightning; climate change; regression analysis; trends; reanalysis data

1. Introduction

Among all convective hazards, large hail is responsible for the largest economic losses (Gunturi and Tippett 2017). Both in Europe and the United States (U.S.), single events causing losses exceeding 1 billion dollars have been recorded (Chagnon et al. 2009; Púčik et al. 2019) and yearly hail losses are estimated between $8-14 billion (Podlaha et al. 2020). Given these large impacts, research has extensively focused on determining the environments conducive to large hail, mapping its occurrence and, at the same, understanding its relationship with climate change.

Hail observations or reports are collected across several regions of the world by voluntary reporters, weather stations or hail pad networks (Allen et al. 2020). The Storm Prediction Center's (SPC) Storm Events dataset (Schaefer and Edwards 1999) includes reports starting in the 1950s, while in Europe, hail reports are stored in the European Severe Weather Database (ESWD; Dotzek et al. 2009; Groenemeijer et al. 2017). Although these databases are an important resource for severe weather research, climatologies exclusively based on ground-based observations are strongly influenced by non-meteorological factors (Allen and Tippett 2015) such as population density variations and associated inhomogeneous reporting rates, or erroneously estimated hail sizes (Witt et al. 2018). Across Europe, there is bias of severe weather reporting towards Central Europe (Groenemeijer and Kühne 2014; Taszarek et al. 2020a), while in the U.S. report-based climatologies

underestimate hailfall across areas with low population density (Blair et al. 2017) such as the High Plains (Wendt and Jirak 2021). Analyses of long-term changes based on such datasets are strongly affected by changes in non-meteorological factors (Schaefer et al. 2004; Doswell et al. 2015), masking the climatological trend.

Remote sensing techniques can overcome the influence of non-meteorological factors. Cintineo et al. (2012) and Wendt and Jirak (2021) developed objective climatologies of large (≥ 2 cm) and very large (≥ 5 cm) hail using the Maximum Estimated Size of Hail (MESH) showing that radar-based proxies can help estimate hail frequency in low populated regions. Although more objective, such climatologies are limited to regions covered by reliable radar networks. In the U.S., where radars cover almost the entire nation, a country-wide climatology can be established, as was done by Murillo et al. (2021). In contrast, in Europe radar parameters from which hail occurrence can be inferred are not exchanged across borders, so that a comparable radar-based hail climatology cannot be developed. Comparable analyses have therefore been limited to a few countries with adequate radar data availability (Nisi et al. 2018; Fluck et al. 2021). Another limitation of radar data is that the time periods for which they are available is too short to investigate long-term trends.

Satellite-based approaches allow for a globally consistent detection of hailstorms and can be used in countries where hail reporting or radar data are sparse or non-existent. They have allowed stochastic catalogues of hailstorms (Punge et al. 2014) across such regions and global hail climatologies (Cecil and Blankenship 2012; Bang and Cecil 2019) to be developed. But satellite-based hail detection methods are limited by the relatively coarse resolution of most satellite-instrumentation compared to the scale of convective phenomena (Bang and Cecil 2019) and by the fact that storm tops detected in infrared and visible imagery only reveal part of what is happening in the cloud. Overshooting Top (OTs) detection using infrared brightness gradients (Bedka et al. 2010) are on their own not sufficient to infer whether hail reaches the ground, especially in regions where substantial hailstone melting below the wet-bulb zero-degree level is likely (Punge et al. 2017). Furthermore, trend analysis is still complicated or impossible for data of many satellite-based sensors, because of their limited time of operation (Murillo et al. 2021).

Environmental based proxies from atmospheric reanalyses can also be used to develop long-term climatologies and study trends. For instance, high CAPE is associated with the occurrence of severe weather and large hail (Craven and Brooks 2004; Groenemeijer and Van Delden 2007; Allen et al. 2015; Lin and Kumjian 2022) and a connection between strong Deep Layer Shear (DLS), the occurrence of supercell-type storms, and hail ≥ 5 cm has been established (Thompson et al. 2012; Johnson and Sugden 2014; Púčik et al. 2015; Taszarek et al. 2020b; Kumjian et al. 2021). Several other atmospheric parameters have skill in predicting the occurrence of hail (e.g., low height of the melting layer; Mahoney et al. 2012; Dessens et al. 2015) or hail size (e.g., high lifting condensation level; Púčik et al. 2015; Taszarek et al. 2020b). Machine learning and statistical approaches indicate that composite parameters that combine together kinematic and thermodynamic parameters were found to correlate well with the occurrence of large hail (Allen et al. 2015; Czernecki et al. 2019; Gensini et al. 2021). Composite parameters such as the Significant Hail Parameter (SHP; http://www.spc.noaa.gov/exper/mesoanalysis/help/help_sigh.html) and the Large Hail Parameter (LHP; Johnson and Sugden 2014) were used to model hail climatologies and study long-term trends (Tang et al. 2019; Taszarek et al. 2020b). Although composite parameters such as SHP perform well across the U.S., climatologies based on SHP tend to produce worse results across regions where the parameter has not been specifically developed (e.g., Europe; Taszarek et al. 2020b).

More elaborated approaches have been taken by Prein and Holland (2018) and Rädler et al. (2019), who used probability density functions and additive logistic regression models, respectively. Their work was based on data from the ERA-Interim reanalysis (Dee et al. 2011) with spatial and temporal resolutions of 6 hours and 0.75° degrees. The spatial resolution of ERA-Interim limited these authors in modelling accurately the frequency of hail in regions of complex orography, where mesoscale circulations can amplify or suppress hail occurrence (Nisi et al. 2016, Kunz et al. 2017). A challenge of reanalysis-based approaches is to accurately account for the failure of storm development in otherwise favorable conditions for large hail, which, when neglected may lead to

Preprints (www.preprints.org) | NOT PEER-REVIEWED | Posted: 3 August 2023 doi:10.20944/preprints202308.0314.v1

overestimation wherever strong convective inhibition commonly occurs. Rädler et al. (2019) therefore treated separately the probability of convective initiation and the probability of large hail given that a storm would develop. Their model resulted in a reasonable depiction of the spatial distribution and annual cycle of hail and predicted that conditions for large hail had become more favorable across Central Europe since 1979, being forced primarily by rising lower-tropospheric moisture and CAPE in response to rising temperatures.

Here we build on the work by Rädler et al. (2019) but make use of full model-level data of the ERA5 reanalysis (Hersbach et al. 2020) at 1 hour and 0.25° resolution. We complement the study from Taszarek et al. (2021b) of convective parameter evolution across Europe and the U.S. since 1979 by using a trained probabilistic logistic model to model the frequency of a specific hazard, i.e., large hail, while simultaneously extending the analysis back to 1950, yielding a 72-year period. Compared to Rädler et al. (2019), who used a very limited number of vertical levels, the ERA5 model-level data used here allow for a much wider choice of derived parameters to be tested as candidate predictors for the model. For instance, we can now test how the vertical distribution of CAPE in the storm affects the probability of large hail, which is interesting given recent findings from Lin and Kumjian (2022) suggesting that (given enough CAPE) hail grows larger with less buoyancy in the low levels. In a similar way, we can test which measure of vertical wind shear has the greatest predictive skill for large hail occurrence. In addition, the improved vertical resolution can be expected to yield more accurate estimates for quantities like low-level moisture, low-level wind shear, and convective inhibition, while the higher spatial resolution of the ERA5 reanalysis data can better reflect the modulation of environmental parameters near orography. Finally, compared to Rädler et al. (2019) we here develop logistic models up to 4 predictors, compared to the 2 used by them.

The three main goals of this study, therefore, are to find better predictors for large hail occurrence, to develop a climatology with higher spatial resolution, and extend the trend analysis further back than has been possible up until now.

2. Data

We used three types of data: lightning observations, hail reports, and convective parameters from the ERA5 reanalysis. The lightning observations and hail reports were gridded onto a 0.25° × 0.25° horizontal grid and were rounded down to the full hours to allow for direct comparison with the reanalysis at the same resolution. For instance, a report occurring at 19:40 UTC was rounded down to 19:00 UTC allowing to sample the pre-convective environment as done by Rädler et al. (2019). Data were derived for the domains presented in Figure 1.

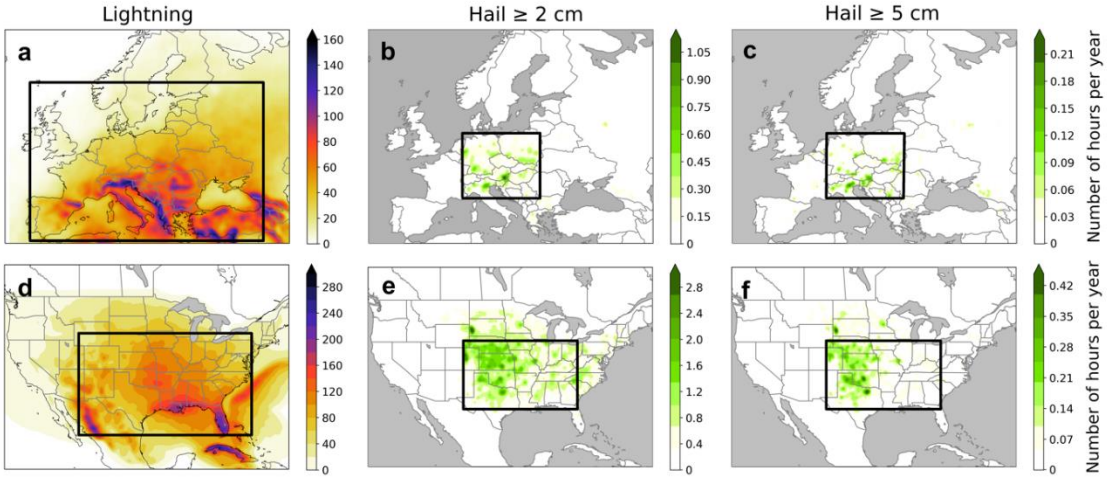

Figure 1. Annual mean distribution of lightning (**a, d**), hail ≥ 2 cm (**b, e**) and hail ≥ 5 cm (**c, f**), Across Europe, the annual mean refers to the period 2008–2020 while across the U.S. to 2010–2020. The black squares highlight the training regions for the different hazard models: lightning Europe (34.5° –

 doi:10.20944/preprints202308.0314.v1

63.5°N, -9.0° – 46.0°W), lightning U.S. (29.0° – 41.5°N, -109.0° – -79.0°W), hail Europe (45.0° – 54.0°N, 5.0° – 22.0°W), hail U.S. (30.5° – 41.5°N, -105.0° – -82.0°W).

a. Lightning detection data

Across Europe, lightning detection data from the Arrival Time Difference Network (ATDnet; Anderson and Klugmann 2014; Enno et al. 2020) were used. This network can detect cloud-to-ground lightning flashes and, to lesser extent, intracloud flashes even at large distances from a sensor. Before 2008, the network was subject to several upgrades that improved the detection efficiency (Enno et al. 2020). To avoid any impacts of such changes, only data between 2008 and 2020 were used. Across the U.S., lightning detection data from the National Lightning Detection Network (NLDN; Koehler 2020) were used for the period 2010–2020. Following Rädler et al. (2019), we defined a lightning case as a one-hour period with at least 2 lightning strikes per grid box (0.25° × 0.25°), primarily to avoid situations with erroneous single detections.

The spatial distribution of lightning correlates well with orographic features in Europe with maxima near the main mountain ranges of the Alps, Caucasus, Apennines, Carpathians, and Pyrenees (Figure 1). The highest number of lightning hours (around 160 per year) is observed along the southern Alpine range, in north-eastern Italy. In the U.S., thunderstorms are more frequent than in Europe, especially in Florida and the Southeast where annual averages exceed 200 lightning hours.

b. Hail reports

For Europe, hail reports were obtained from the European Severe Weather Database (ESWD; Dotzek et al. 2009; Groenemeijer et al. 2017) for the period 2008–2020 and organized into two categories: large hail, with a maximum dimension larger than 2 cm, and very large hail, with a maximum dimension larger than 5 cm. Like Rädler et al. (2019), reports with a time uncertainty of more than 1 hour were discarded. Over Europe, the spatial distribution of (very) large hail reports (Figure 1b, c) features maxima across northern Italy, south-eastern Austria, and southern Poland. The dataset does not fully reflect true hail occurrence, because reporting rates vary and have a bias towards Central Europe (Groenemeijer et al. 2017; Taszarek et al. 2020a). The training region for the hail model was constrained to areas of relatively frequent and homogenous reporting (boxes in Figure 1b, c) and is therefore smaller than that for the lightning model (box in Figure 1a).

In the U.S., hail data from the SPC Storm Events dataset (Schaefer and Edwards 1999) was used for the period 2010–2020. The spatial distribution of hail reports strongly depends on hail size (Figure 1e, f). While hail ≥ 2 cm is most common across the Plains, and to a lesser extent the Midwest and the East coast states, hail ≥ 5 cm occurs almost exclusively in the High Plains in the lee of the Rocky Mountains. Like in Europe, the influence of population density on hail report density is clear, since metropolitan areas such as Oklahoma City, Dallas-Fort Worth, and Denver stand out clearly (Figure 1e, f).

c. Reanalysis

Reanalysis data were used here for two purposes: first to define best lightning and hail predictors for the logistic model development and second to reconstruct climatologies and corresponding long-term trends for the period of 72 years (1950–2021). We used the fifth generation European Centre for Medium Range Weather Forecasts (ECMWF) atmospheric reanalysis (ERA5; Hersbach et al. 2020). ERA5 has a 0.25° horizontal grid spacing with 137 terrain-following hybrid-sigma model levels and an hourly resolution. 172 convection related parameters were computed using the *thundeR* R language package (Taszarek et al. 2021b), a selection of which was considered as candidate predictors (Appendix A). The parameters include commonly used metrics for hail forecasting such as CAPE, DLS and Storm Relative Helicity (SRH). In addition, we calculated new parameters related to buoyancy to investigate if their predictive skill for the occurrence of lightning and hail would be higher compared to their conventional variants. New parameters related to buoyancy include the CAPE above the -10°C level, selected as a proxy of the updraft strength in the top portion of the storm, and the CAPE for a source parcel originating above 500 m AGL, which was

Preprints (www.preprints.org) | NOT PEER-REVIEWED | Posted: 3 August 2023 doi:10.20944/preprints202308.0314.v1

chosen to eliminate the possible selection of a near-surface parcel not representative of the storm inflow.

2. Model development

a. Model setup

We developed Additive Logistic Regression Models that, once trained with lightning observations and hail reports, yield a probability of hail (or lightning) as a function of the values that each of the predictor parameters from the atmospheric reanalysis take at any grid point at a given time. We followed Rädler et al. 2019 who named the resulting models Additive Regression Convective Hazard Models (AR-CHaMo). The probability of hail ≥ 2 cm $P_{\text{hail}\geq 2\text{cm}}$ at a given time and place is computed as the product of the probability of a thunderstorm occurring $P_{\text{lightning}}$ and the conditional probability of hail given a storm $P_{\text{hail}\geq 2cm\,|\,\text{lightning}}$:

$$P_{\text{hail}\geq 2\text{cm}} = P_{\text{lightning}} \cdot P_{\text{hail}\geq 2\text{cm}\,|\,\text{lightning}}$$

To sample the pre-convective environment, the models were developed using ERA5 conditions sampled one hour before the lightning and hail reports occurred, as done by Taszarek et al. (2020b). Compared to Rädler et al. (2019), the model training regions were significantly extended. This, summed with the high spatio-temporal resolution of the ERA5 reanalysis, resulted in a high number of data points being sampled to train the logistic models, more than a billion for the Europe lightning model (Table 1).

Table 1. Number of data points, events, and ratio of events to all data points for lightning, hail ≥ 2 cm and hail ≥ 5 cm models. The number of hail ≥ 2 cm and hail ≥ 5 cm events occurring in presence with lightning is shown in brackets.

	Number of data points		**Number of events**		**Ratio**	
	Europe	U.S.	Europe	U.S.	Europe	U.S.
Lightning	1 607727264	882965952	10872890	13088628	0.68 %	1.48 %
Hail ≥ 2 cm*	1710071	5678261	5879 (5493)	39619 (38516)	0.32 %	0.10 %
Hail ≥ 5 cm*	1710071	5678261	848 (805)	3789 (3723)	0.05 %	0.07%

* Only reports in the presence of lightning within 1 hour and 50 km (in brackets) were considered within the training dataset.

b. Model selection

The Deviance Explained (Wood 2006) and the Bayesian Information Criterion (BIC; Schwarz 1978) scores were used for model selection, i.e., to choose the explanatory variables from the selection of candidate predictor parameters. The Deviance Explained, defined as the proportion of null deviance explained by the model, was used to compare the skill of models with the same number of predictors (the higher, the better) as done by Knaff et al. (2018) and Rädler et al. (2019). The BIC score is computed using the logarithm of the maximized value of the likelihood function of the model and a penalty term for the number of parameters fitted (Wilks 2006). The BIC was taken in consideration to prevent overfitting when comparing models with different number of predictors (the lower, the better). The predictive skill of an n+1 dimensional model is higher only if the deviance explained is higher and the BIC is lower than that of an n dimensional model.

 doi:10.20944/preprints202308.0314.v1

The parameter selection procedure was streamlined using prior knowledge of the basic ingredients of convection for both the hail and the lightning models. Starting with the lightning model, according to Doswell et al. (1996), three ingredients are required for a convective storm to form: conditional instability, moisture, and lift. We have used this notion to eliminate the need for testing all possible combinations of 172 predictors. Following results from Westermeyer et al. (2017) and Poręba et al. (2022), instability and mid-level relative humidity measures were first used to build a 2-dimensional lightning model, before subsequently improving it by including other parameters relevant for convective initiation. More precisely we followed these steps:

- Divide convective-initiation relevant parameters from ERA5 into three main categories: "instability", "humidity" and "other" parameters relevant for convective initiation.
- Develop a 2-dimensional model by choosing the "instability" - "humidity" parameter combination yielding the highest predictive skill.
- Test adding "other" parameters to the initial 2D model. The parameter adding the most skill is chosen.
- Repeat the previous step until adding parameters results in an increasing BIC score.

The procedure yielded a 5-dimensional model with the same predictors when followed for the European and the U.S. data.

A similar approach was followed for the development of the models for the conditional probability of (very) large hail. Here, we have taken into account the notion that vertical wind shear enhances large hail probability (Allen et al. 2015; Púčik et al. 2015; Dennis and Kumjian 2017; Kumjian and Lombardo 2020; Taszarek et al. 2020b; Gensini et al. 2021) and therefore use instability in combination with shear-related parameters (instead of "humidity") to build a base two-dimensional model, before adding "other" parameters (relevant for large hail) according to the procedure described above. A full list of all tested parameters under each category ("instability"," humidity","shear", "other") for both the lightning and hail models is shown in Tables A1 and A2, respectively. The final predictors selected following this procedure are listed in Table 3.

c. Regional differences in instability-shear parameter performance for conditional hail models

The Europe and the U.S. models were developed under the hypothesis that convective storms require the same ingredients regardless of the geographical region where they form, as they are controlled by the same physical processes. This, however, does not mean that predictor parameters are equally skillful in every region or subregion. For example, if a lack of wind shear is the limiting factor for hailstorm development in one region, wind shear will be a good discriminator between situations with and without hail there, while in another region where wind shear is ubiquitous, but a lack of instability limits hailstorm development, it may be a poor predictor. While developing the conditional hail models, we found the skill of predictors that represent instability to differ substantially geographically (Table 2). The difficulty to find a skillful predictor for both Europe and the different regions of the U.S. is supported by findings from Zhou et al. (2021) who showed that the conditions supportive for hailstorms are highly geographically dependent. While in Europe CAPE variants are most skillful, mid-level temperature lapse rates discriminate better between hail and non-hail situations in the U.S. CAPE is a particularly poor predictor of hail in the U.S. Southeast (Figure 2b). Here, sizable CAPE is common, but often occurs with modest vertical lapse rates and with a moist lower troposphere that promotes high condensate loading. This combination negatively affects the probability of hail, since relatively weak convective updrafts with modest parcel buoyancy occur under such circumstances according to cloud model simulations (Storer and van den Heever 2014; Kirkpatrick et al. 2009).

Preprints (www.preprints.org) | NOT PEER-REVIEWED | Posted: 3 August 2023 doi:10.20944/preprints202308.0314.v1

Table 2. Deviance explained (higher values are better) for a selection of instability and shear candidate predictor parameters for large (≥ 2 cm) hail across Central Europe, the U.S., and two U.S. subregions, the Southeast and the Southern Plains. The acronyms are explained in the text and in Tables A1, A2 which include a list of all tested predictor parameters for the lightning, hail ≥ 2 cm and hail ≥ 5 cm models.

	Central Europe	U.S.	U.S. Southeast	U.S Southern Plains
	Deviance explained (%)			
MU_CAPE	6.38	4.54	2.02	7.35
ML_CAPE	6.26	3.25	0.80	5.67
SB_CAPE	6.39	2.96	0.60	5.97
MU_LI	6.11	3.91	1.98	5.87
MU_CAPE_HGL	5.99	2.77	0.90	4.76
MU500_CAPE	6.26	5.94	3.45	7.69
MU_CAPE-10°	7.34	7.01	6.04	9.15
MU500_CAPE-10°	7.43	7.28	6.35	9.95
LR_3-6km	1.50	6.86	6.17	5.57
BS_0-6km	1.39	4.10	4.12	3.47
EFF_MU_BS	4.81	6.84	5.49	6.53

Preprints (www.preprints.org) | NOT PEER-REVIEWED | Posted: 3 August 2023 doi:10.20944/preprints202308.0314.v1

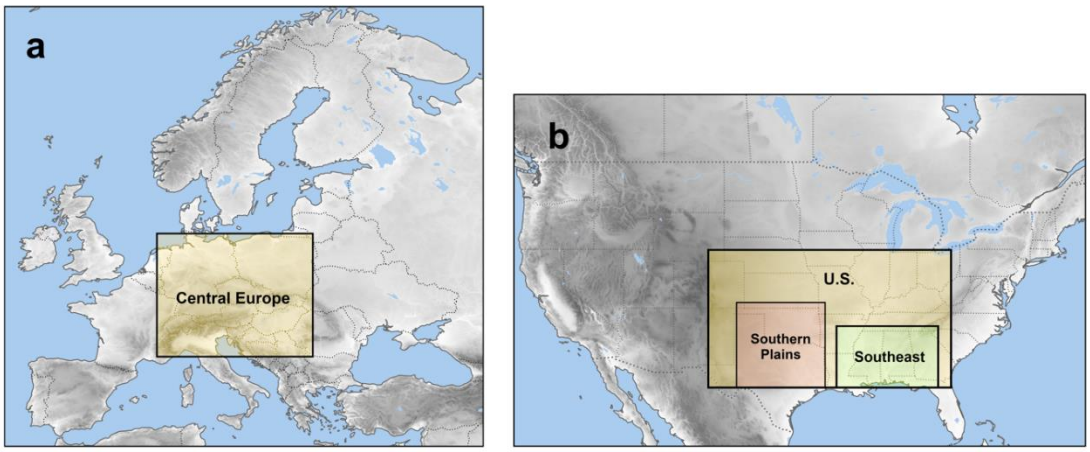

Figure 2. Training region for hail ≥ 2 cm and hail ≥ 5 cm for **(a)** Europe and **(b)** the U.S. Across the U.S. the hail models were tested also across two sub-regions: the Southern Plains (30.00° – 38.00°N, 94.25° – 102.50° W) and the Southeast (29.25° – 36.00°N, 83.00° – 93.25° W).

We investigated variants of CAPE to find a better predictor for large hail. First, CAPE for the most-unstable parcel (defined as the one with the highest theta-e value in the 0–3 km AGL layer) originating above 500 m AGL (MU500_CAPE) was tested. This was done to eliminate the possibility of a very shallow near-surface layer, unrepresentative of the storm inflow, to be selected as source of the lifted parcel. Although this variant outperformed standard MU_CAPE, across the U.S. Southeast it still had considerably lower skill than other instability-related parameters such as the Lapse Rates between 3 and 6 km (LR_3–6km) AGL. Possibly, large hail in the Southeast is strongly tied to the presence of an Elevated Mixed Layer (EML) as this results in a lower fraction of the CAPE being released in the bottom portion of the updraft - which Lin and Kumjian (2022) show to favor large hail growth. Next, we tested parameters that consider the amount of CAPE in the cold, upper, portion of the storm. CAPE released in the hail growth layer (CAPE_HGL; between the -10°C and -30°C isotherms; Knight and Knight 2005) was tested but yielded a lower predictive skill than MU_CAPE (Table 1). MU_CAPE in the layer above the -10 °C isotherm (MU_CAPE-10°), more specifically the variant computed for the most unstable parcel above 500 m (MU500_CAPE-10°), stood out as the best instability predictor across Europe, the U.S., and its subregions. This universal skill in both continents suggests that it may better represent what is relevant for hail formation, i.e., large buoyancy high in the storm.

A similar comparison of the skill of shear-related parameters was carried out. In contrast to instability parameters, little variation in skill was found between different geographical regions. Overall, the Effective Most Unstable Shear (EFF_MU_BS) was the best shear parameter, outperforming bulk wind shear between 0 and 6 km AGL (BS_0–6 km). EFF_MU_BS is the bulk wind shear between the height of the most unstable parcel origin and halfway to its Equilibrium Level, similar to Thompson et al. (2007) but without assuming an effective-inflow layer.

d. Final models and their validation

The predictor parameters for the lightning, hail ≥ 2 cm and hail ≥ 5 cm models are shown in Table 3.

Preprints (www.preprints.org) | NOT PEER-REVIEWED | Posted: 3 August 2023 doi:10.20944/preprints202308.0314.v1

Table 3. Selected predictor parameters for the regression models. The acronyms are explained in the text.

Model	Lightning	Hail ≥ 2 cm	Hail ≥ 5 cm
Predictors	MU_LI (K)	MU500_CAPE-10° (J kg^{-1})	MU500_CAPE-10° (J kg^{-1})
	RH_500–850hPa (%)	EFF_MU_BS (m s^{-1})	EFF_MU_BS (m s^{-1})
	1h Acc. Conv. Precip. (kg m^{-2})	ML_MIXR (g kg^{-1})	ML_MIXR (g kg^{-1})
	MU MIXR (g kg^{-1})	0° height (m)	ML_LCL height (m)
	Land-sea Mask		

The base 2-dimensional model for lightning was developed using the Most Unstable Lifted Index (MU_LI) defined as by Galway (1956) and the average relative humidity between 500 and 850 hPa (RH_500–850hPa). MU_LI and RH_500–850hPa represent two crucial ingredients for convective initiation: instability and mid-level moisture, as shown by Rädler et al. (2019) using ERA-Interim. The model with CAPE, instead of MU_LI, performed worse (deviance explained 28.0% against 30.1% of the MU_LI model) and was found to underestimate lightning across mountainous regions whereas the MU_LI model suffers less from this bias (e.g., across the Atlas Mountains and the Spanish Plateau in Europe). While CAPE by itself can only quantify positive buoyancy, LI is a continuous quantifier regardless of stability (Púčik et al. 2017; Pilguj et al. 2022). This may make LI more suitable in a logistic model which needs to represent accurately whether low amounts of instability are or are not sufficient to support lightning.

Convective precipitation added the most skill (deviance explained: 32.5%, BIC $3.05 \cdot 10^6$) to this initial 2-dimensional model (deviance explained: 30.1%, BIC $3.16 \cdot 10^6$), arguably because it distinguishes situations with convective inhibition despite sufficient instability and moisture. It is a common parameter in modelling studies using reanalyses and climate projections (Trapp et al. 2009; Tippett et al. 2012; Romps et al. 2014; Allen and Tippett 2015; Púčik et al. 2017; Tippett et al. 2019; Taszarek et al. 2021a). The fourth parameter is mixing ratio for the most unstable parcel (MU_MIXR). The probability of lightning is bimodally distributed as a function of MU_MIXR (not shown): given sufficient instability and mid-level moisture, lightning probability increases with increasing MU_MIXR up to 12–15 g/kg, depending on the amount of instability (higher for more unstable environments), and then decreases again. Possibly, the probability of storm electrification is suppressed by excessive water loading in very moist environments. The inclusion of MU_MIXR reduced the frequency of lightning across the Gulf of Mexico (not shown). Finally, a land-sea-mask was added to reflect the observation that lightning is less common over the sea than over land, which may be attributed to other parameters not explored here, e.g., aerosol load or LCL height (Williams and Stanfill 2002; Romps et al. 2018).

The hail ≥ 2 cm and hail ≥ 5 cm model each have four predictors and share three of them, i.e., MU500_CAPE-10°, EFF_MU_BS, and ML_MIXR. The fourth predictor giving most additional skill differs between the two models. For hail ≥ 2 cm, it is the height of the 0° isotherm while, for hail ≥ 5 cm, it is the height of the Lifting Condensation Level for the mixed layer (0–500 m AGL) parcel (ML_LCL). ML_LCL lends the additional skill to the model for hail ≥ 5 cm because for the same amount of instability, high cloud bases are associated with stronger and wider updrafts which favor the development of very large hailstones (McCaul and Weisman 2001, Mulholland et al. 2021). On the other hand, for smaller hailstones, which are more sensitive to melting (Rasmussen and Heymsfield 1987; Kumjian et al. 2019), the height of the wet-bulb zero degree level is more important.

The performance of the models can be quantified by the Area Under the ROC Curve (AUC) score. The lightning (EU: 0.943 and U.S: 0.931), hail ≥ 2 cm (EU: 0.983, U.S: 0.964) and hail ≥ 5 cm (EU: 0.989, U.S: 0.979) models are all highly skillful. A further investigation of the robustness of the models was carried out by training the models on even year data across each region and, subsequently, generating predictions for odd years. The performance of the models was similar to the full year

Preprints (www.preprints.org) | NOT PEER-REVIEWED | Posted: 3 August 2023 doi:10.20944/preprints202308.0314.v1

models (lightning EU: 0.939, lightning U.S: 0.926; hail ≥ 2 cm EU: 0.977, hail ≥ 2 cm US: 0.961; hail ≥ 5 cm EU: 0.981, hail ≥ 5 cm U.S: 0.973). These findings suggest that the AR-CHaMo models are robust. The performance of the 4-dimensional conditional hail models was also compared with that of a logistic model based on SHP (Table 4). The AR-CHaMo hail outperformed SHP for both hail sizes and regions showing that it discriminates hail and non-hail environments better than SHP.

Table 4. AUC scores for hail ≥ 2 cm and hail ≥ 5 cm models given convective initiation. The performance of AR-CHaMo is compared with that of a logistic model based on SHP.

	Europe		**U.S.**	
	AR-CHaMo	SHP	AR-CHaMo	SHP
Hail ≥ 2 cm	0.778	0.764	0.764	0.739
Hail ≥ 5 cm	0.894	0.865	0.878	0.819

4. Modelled lightning and its evolution since 1950

a. Mean distribution

Modelled annual and seasonal lightning distributions from AR-CHaMo are compared to lightning observations across Europe and the U.S. by constraining the modelled data to the period for which lightning observations are available, i.e., 2008-2020 (2010-2020) across Europe (U.S.).

In Europe, the annual mean modelled distribution reflects the observed spatial patterns well (Figure 3). Both the model and the observations highlight maxima across mountainous areas, especially the Alps and the Caucasus. Although coastal areas also stand out as local maxima in the model output, lightning is underestimated across the Balkans and the southern Mediterranean coasts (especially Turkey). The seasonal cycles match well: in winter, the occurrence of convective storms is limited to the south-eastern Mediterranean. During spring, the storm activity picks up over the continent, more rapidly across Eastern Europe and Turkey where a seasonal maximum is present. Lightning is most common during the summer over the continent where a band of lightning activity stretches from the Pyrenees across Central Europe to Russia. Although the model accurately reproduces such spatial feature, it underestimates the activity across parts of south-eastern Europe. Finally, in autumn the peak in the activity shifts to the relatively warm waters of the southern Mediterranean and the surrounding coastal regions where the model underestimates the activity compared to the observations.

Preprints (www.preprints.org) | NOT PEER-REVIEWED | Posted: 3 August 2023 doi:10.20944/preprints202308.0314.v1

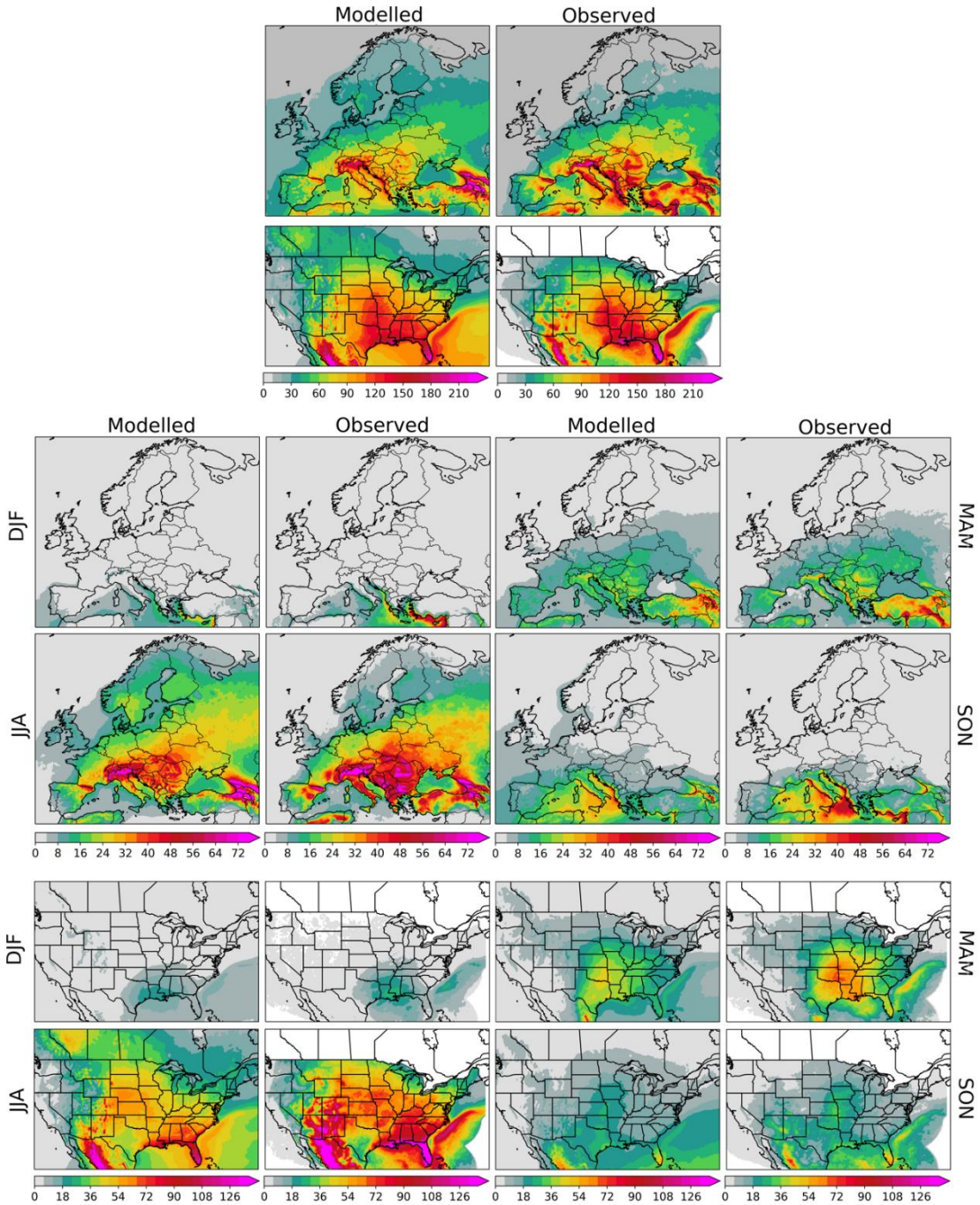

Figure 3. Mean annual and seasonal number of hours with lightning from model and observations. Data refers to the period 2008-2020 across Europe and to the period 2010-2020 across the U.S.

Across the U.S., a maximum in lightning occurrence is modelled across southern Louisiana and Florida, part of a large region with high thunderstorm activity that extends from the Southeast U.S. into the Central Plains. The spatial distribution of lightning is less influenced by orography than in Europe but does play a role in the Southwest, where local maxima correspond to mountain ranges. Along the Gulf of Mexico coast, a sharp land-sea contrast exists with less lightning over sea than over the surrounding land. The model underestimates lightning across the Southeast, Florida, and the mountains of the Southwest. The modelled seasonal cycle reflects the observed one rather well: in winter, the occurrence of convective storms is limited to the Southeast while in Spring it peaks over the southern Great Plains. The occurrence is underestimated during summer when the observed occurrence peaks higher over Florida and the Southwest. A decrease in occurrence is modelled and observed during Autumn.

Preprints (www.preprints.org) | NOT PEER-REVIEWED | Posted: 3 August 2023 doi:10.20944/preprints202308.0314.v1

The modelled and observed seasonal cycle can be compared quantitatively by averaging over the training region (Figure 4). In Europe, the number of hours of lightning matches the observations almost perfectly in all months apart from May, June, and July when the model slightly underestimates the lightning activity (Figure 4a). In the U.S., lightning activity is somewhat underestimated by the model throughout the year (Figure 4d), but the seasonal cycle is modelled well quantitatively.

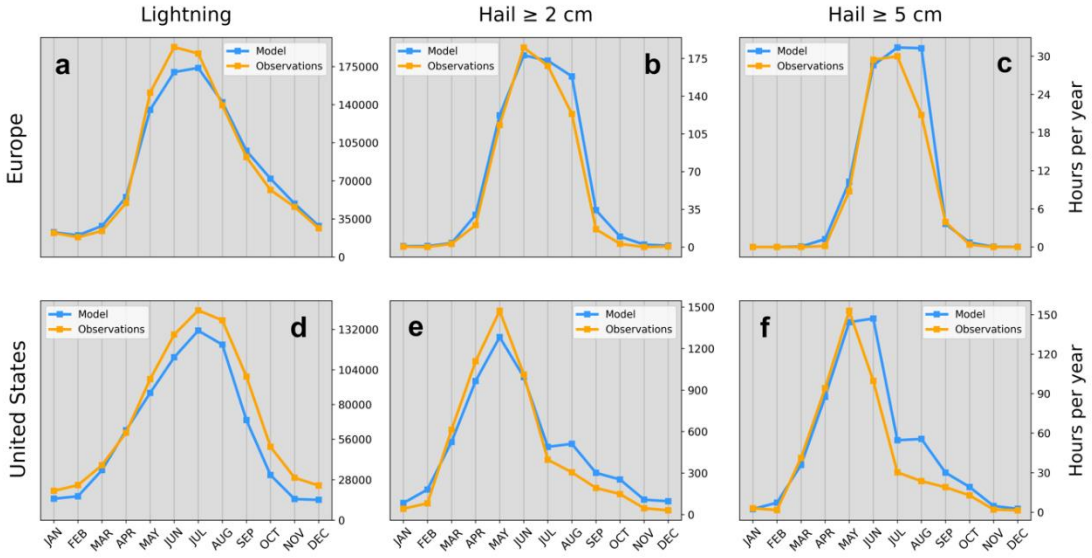

Figure 4. Comparison between modelled and observed seasonal cycles for lightning **(a,d)**, hail ≥ 2 cm **(b,e)**, hail ≥ 5 cm **(c,f)** across Europe and U.S. training regions.

b. Long-term trends

AR-CHaMo suggests that the occurrence of thunderstorm environments has significantly increased across most of Europe during the past 72 years (Figure 5). The strongest absolute upward trends are found over the Alpine and Caucasus Mountain ranges with an increase up to 5 hours of lightning more per decade. Scandinavia stands out as the region with the largest relative increases with 2 more hours per decade while the annual mean is 20–25 hours. These increases in lightning occur throughout the year, but especially in the summer. In a belt from Finland to Turkey, small, statistically insignificant changes are modelled. Across parts of Russia, AR-CHaMo indicates a significant decrease in thunderstorms. Some significant trends are also observed in areas with very low absolute values, which are displayed in white. These findings are consistent with Taszarek et al. (2021a), however, their analysis was limited to the period 1979–2021. For direct comparison, figures for the same period are included in Appendix B.

Preprints (www.preprints.org) | NOT PEER-REVIEWED | Posted: 3 August 2023 doi:10.20944/preprints202308.0314.v1

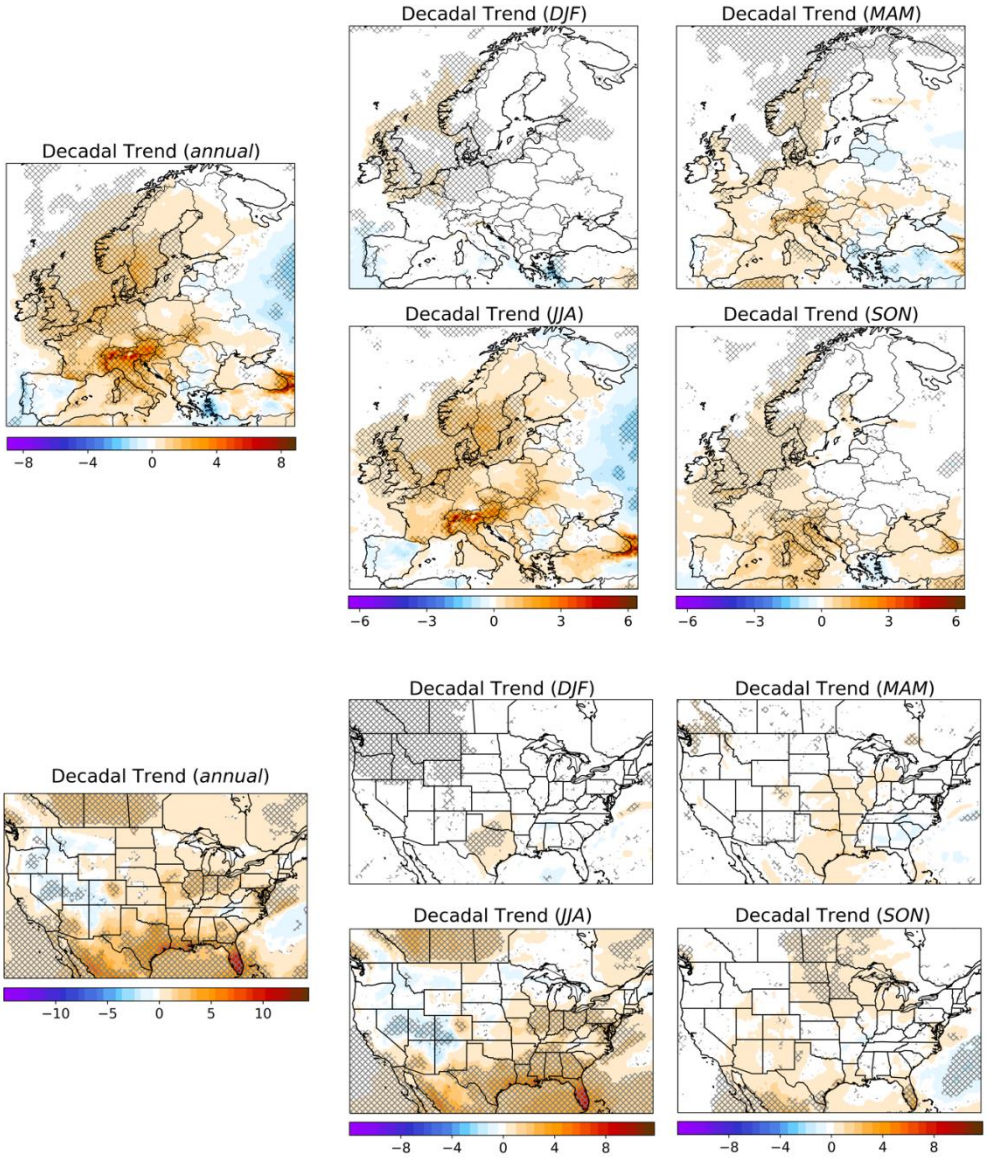

Figure 5. Annual and seasonal trends in lightning hours across Europe and the U.S. between 1950 and 2021. Values are expressed as the change in the number of hours per decade. Trends significant at a 95th percentile level are hatched.

The strongest positive trends in the U.S. occur in the southern states, specifically Florida and the Texas-Louisiana coasts. Although not as strong, upward trends can also be found in the Midwest and across southern Canada, mostly during summer. Conversely, a region of significant negative trends is located across the Colorado Plateau and the Great Basin.

When comparing the trends in Figure 5 with those found by Taszarek et al. (2021b), there are a number of similarities and differences. We do not find any strong negative trends across the southern Great Plains. There are two possible reasons for this: the difference in the definition of favorable thunderstorm environments and the difference of period for which the trends were calculated with Taszarek et al. (2021b)'s analysis starting in 1979. Indeed, when constraining the trend analysis with AR-CHaMo to the period 1979–2021 (Appendix B) similar patterns to Taszarek et al. (2021b) result, i.e., negative trends across most of the southern Great Plains and the Southwest. Nonetheless, some differences between the two approaches remain, especially across the Gulf Coast, probably because of the different lightning proxies used, i.e., AR-CHaMo versus those of Taszarek et al. (2021b).

Preprints (www.preprints.org) | NOT PEER-REVIEWED | Posted: 3 August 2023 doi:10.20944/preprints202308.0314.v1

5. Modelled hail ≥ 2 cm and hail ≥ 5 cm and their evolution since 1950

a. Europe

Hail ≥ 2 cm is most frequent in the Po Valley in northern Italy, averaging to around one event per year (per grid point) while south-western France, eastern and northern Spain also exhibit a relatively high frequency of occurrence (Figure 6). The modelled spatial distribution in Italy accurately reflects that of observed data with a maximum in the northeast (Figure 1b, c), but the maxima in France and Spain are not confirmed by ESWD reports, likely because of the lower reporting rate in those countries (Groenemeijer et al. 2017; Taszarek et al. 2020a). Nonetheless, the spatial distribution across these regions corresponds with that of local hail climatologies based on hail pad network data (Vinet 2001; Merino et al. 2014). Here, the model correctly simulates hail maxima outside of the region where it was trained.

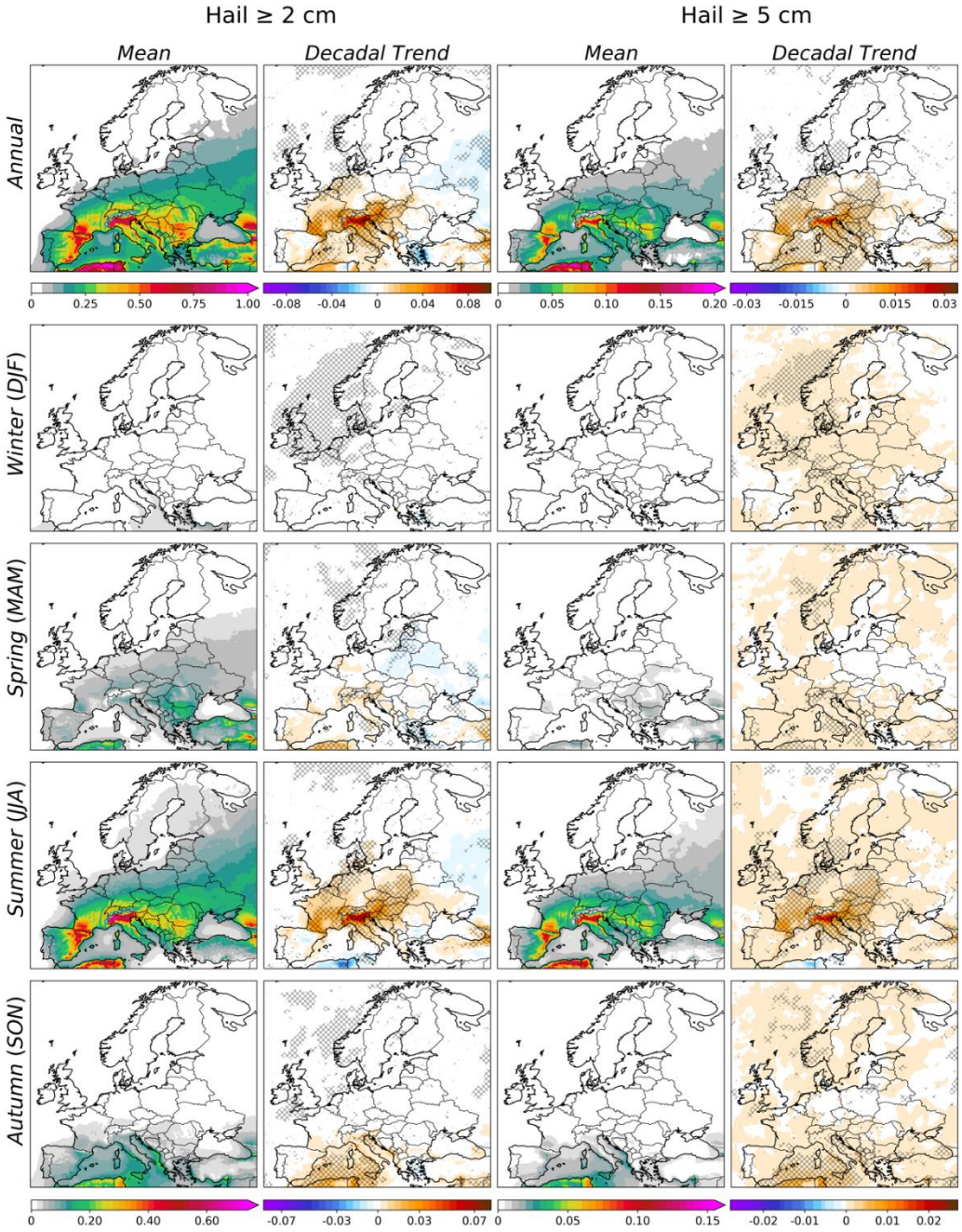

Figure 6. Mean modelled annual and seasonal number of hail hours (hail ≥ 2 cm and hail ≥ 5 cm) between 1950 and 2021 across Europe. Annual and seasonal trends are also shown and expressed as

the change in the number of hail hours per decade. Trends significant at a 95th percentile level are hatched.

Compared to the earlier hail hazard maps from Rädler et al. (2019) based on ERA-Interim, local patterns are much better resolved, especially near complex orography, such as the local maxima across Switzerland and Southern Germany, where the model output is consistent with high resolution climatologies based on radar and observed data (Junghänel et al. 2016; Schrooer et al. 2019). The Atlas region in northern Africa has the highest modelled hail occurrence, which is consistent with the climatology from Punge et al. (2017) that was based on overshooting top detections. The lack of ground-truth observations from this region makes it impossible to verify this prediction but reports of hail ≥ 5 cm are known from this region. For instance, gargantuan hail (Kumjian et al. 2020) with a verified diameter of 17 cm occurred in Libya on the 27th of October 2020 and was reported to the ESWD.

The local maxima of the distribution of hail ≥ 5 cm closely resembles that of hail ≥ 2 cm. Northern Italy and eastern Spain have the highest occurrence in Europe with approximately 1 event every 10 years (per grid box) while northern Africa exhibits the highest frequency overall with about 1 event every five years. Furthermore, northern Africa has the highest ratio of hail ≥ 5 cm to hail ≥ 2 cm environments: one in five hail ≥ 2 cm events involves hailstones with a maximum dimension ≥ 5 cm. This is likely because the environmental conditions that characterise the region, namely steep lapse rates and high LCL favor the genesis of large hailstones (Púčik et al. 2015; Taszarek et al. 2020b; Mulholland et al. 2021).

Hail ≥ 2 cm in Europe occurs mostly in summer, except for parts of the Mediterranean region, such as Turkey, where it is more common in Spring. Although a direct pan-European comparison with observations (Figure 1b, c) is not possible, the modelled climatological spatial distribution is in good agreement with previous studies such as that from Punge et al. (2017), Rädler et al. (2019) and various regional and national climatologies. The modelled seasonal cycles for hail ≥ 2 cm and hail ≥ 5 cm were compared with the observation ones across Central Europe (Figure 4b, c). The model agrees with the observations well especially during Spring and the early summer while a tendency to overestimate the activity is present in August, especially for hail ≥ 5 cm.

The strongest upward and significant trends occur across the Po Valley for both hail ≥ 2 cm and hail ≥ 5 cm, especially in summer, which is in line with Rädler et al. (2019) and Taszarek et al. (2021a). Increases of 0.05–0.08 hours per decade per grid box are modelled, corresponding to a relative increase of approximately 8% per decade. Smaller significant increases are found across France, the Benelux and northern Germany, in Switzerland and Austria, across the north-western Balkans into southern Poland and, further east, across Northeast Turkey and Georgia. Finally, significant positive trends are found in northern Africa during spring and autumn while a decrease in hail activity is modelled in summer. Negative and significant trends are present across the Aegean Sea and parts of western Russia. The trend maps of hail ≥ 2 cm and hail ≥ 5 cm are very similar. The results resemble those of Rädler et al. (2019) in that both studies agree on identifying northern Italy as the region with the strongest positive/significant trends in the occurrence of hail ≥ 2 cm and hail ≥ 5 cm. The largest significant increases of favorable severe thunderstorm environments over northern Italy were also found in Taszarek et al. (2021a).

b. United States

Hail ≥ 2 cm and hail ≥ 5 cm occur more frequently in the U.S. than Europe. A high frequency of occurrence (≥ 2 hours per year) is modelled in the Plains across a region extending from southern Texas northward into Nebraska (Figure 7). While modelled hailfall is less frequent further east, it is still relatively common in states like Wisconsin, Illinois, or Louisiana with an average of 1 hour of hail per year, which is comparable to northern Italy. Compared to hail ≥ 2 cm, hail ≥ 5 cm is more confined to the lee of the Rockies, a feature confirmed by hail observations (Figure 1e, f). For both hail size categories, the maximum in occurrence is in the high Great Plains between south-western Nebraska, north-eastern Colorado, and north-western Kansas. The location of the maximum in

Preprints (www.preprints.org) | NOT PEER-REVIEWED | Posted: 3 August 2023 doi:10.20944/preprints202308.0314.v1

occurrence corresponds with that in the MRMS-MESH based climatology from Wendt and Jirak (2021). Remarkable local features in the hail occurrence pattern occur across eastern Colorado where a marked south to north gradient is modelled or around Rapid City in South Dakota, where a local maximum in occurrence can be distinguished (Figure 7). Both features also exist in hail observations (Figure 1e, f).

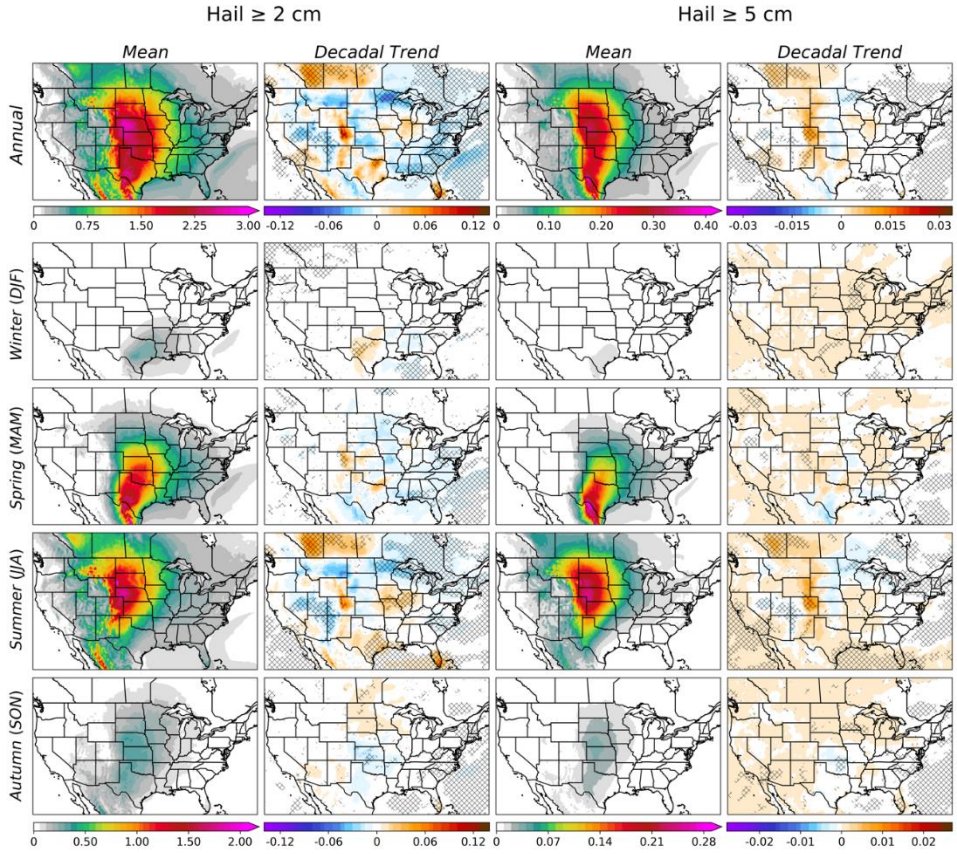

Figure 7. As for Figure 6, but for the U.S. domain.

Unlike Europe, where most of the hail activity is confined to the summer, hail ≥ 2 cm and hail ≥ 5 cm also occur frequently in spring in the U.S. The model reproduces the observed peak in May followed by a rapid decrease in summer (Figure 4). In spring, hail ≥ 2 cm and hail ≥ 5 cm are most common across the southern Great Plains, in particular in Northeast Mexico, Texas and Oklahoma. During summer, hail activity shifts north to the High Plains into southern Canada (specifically around southern Alberta and Saskatchewan) with a maximum across Western Nebraska and South Dakota. A relatively high occurrence is also found in Northwest Mexico across the Western Sierra Madre Mountains, but this is mostly limited to hail ≤ 5 cm.

In the U.S., there are no large areas with positive (significant) trends comparable to those found in Europe. For hail ≥ 2 cm, modest positive statistically significant trends are present in summer across northern Colorado, southern Florida, and southern Canada with the latter two exhibiting the largest relative increases. Weak increases also occurred over western Texas in winter and north-eastern Colorado in spring. A decrease of hail ≥ 2 cm is modelled across the Southeast as also shown by Brimelow et al. (2017), the upper Midwest, the Colorado Plateau, and the Great Basin. In contrast to hail ≥ 2 cm, hail ≥ 5 cm did not decrease significantly across the Southeast and the upper Midwest. These findings contrast with results from Taszarek et al. (2021b) who identified strong positive and significant trends in 99.9th percentile of SHP and the Supercell Composite Index (SCP) and Tang et al. (2019) who find increases in both the LHP and SHP across much of the Central U.S. since 1979. When constraining the analysis to the period starting in 1979, the modelled trends display a more similar pattern to those studies based on SHIP, LHP and SCP (Appendix B), but the match is not

Preprints (www.preprints.org) | NOT PEER-REVIEWED | Posted: 3 August 2023 doi:10.20944/preprints202308.0314.v1

perfect, likely because these parameters, do not take storm initiation into account which AR-CHaMo suggest has become less likely across the Rocky Mountains and the southern High Plains (Figure A2).

6. Evolution of hail and lightning in two hail-prone regions: northern Italy and Oklahoma

A year-by-year comparison from 1950 to 2021 can reveal more details about the nature of the changes across two hail prone areas: northern Italy and central Oklahoma. We do this by using 72 colored stripes whose color represents the percentual departure of each year from the 1950–2021 average, similar to the Warming Stripes by Edward Hawkins (2018) (Figure 8). The modelled frequency of lightning has increased substantially across northern Italy over the last two decades: from 2006 onward, all years except one were above the long-term average. The comparison between observations and model in Figure 9 shows that AR-CHaMo can accurately reproduce the year-to-year variability across the region. The long-term trend (1950–2021) of lightning frequency is +3.4 hours per decade, significant with p-value: < 0.01 using a Wald Test. The rate of increase doubles in the period 1979–2021: +6.8 hours per decade (p-value: < 0.01). Of all predictor parameters, the increase in lightning frequency is most strongly correlated with MU_MIXR (r: 0.80, p-value < 0.01) and MU_LI (r: -0.84, p-value < 0.01) (Appendix C). This confirms that the upward trend in lightning activity is mostly caused by an increase in low-level moisture, leading to increased buoyancy, as reported by Rädler et al. (2019), Taszarek et al. (2021a), and Pilguj et al. (2022).

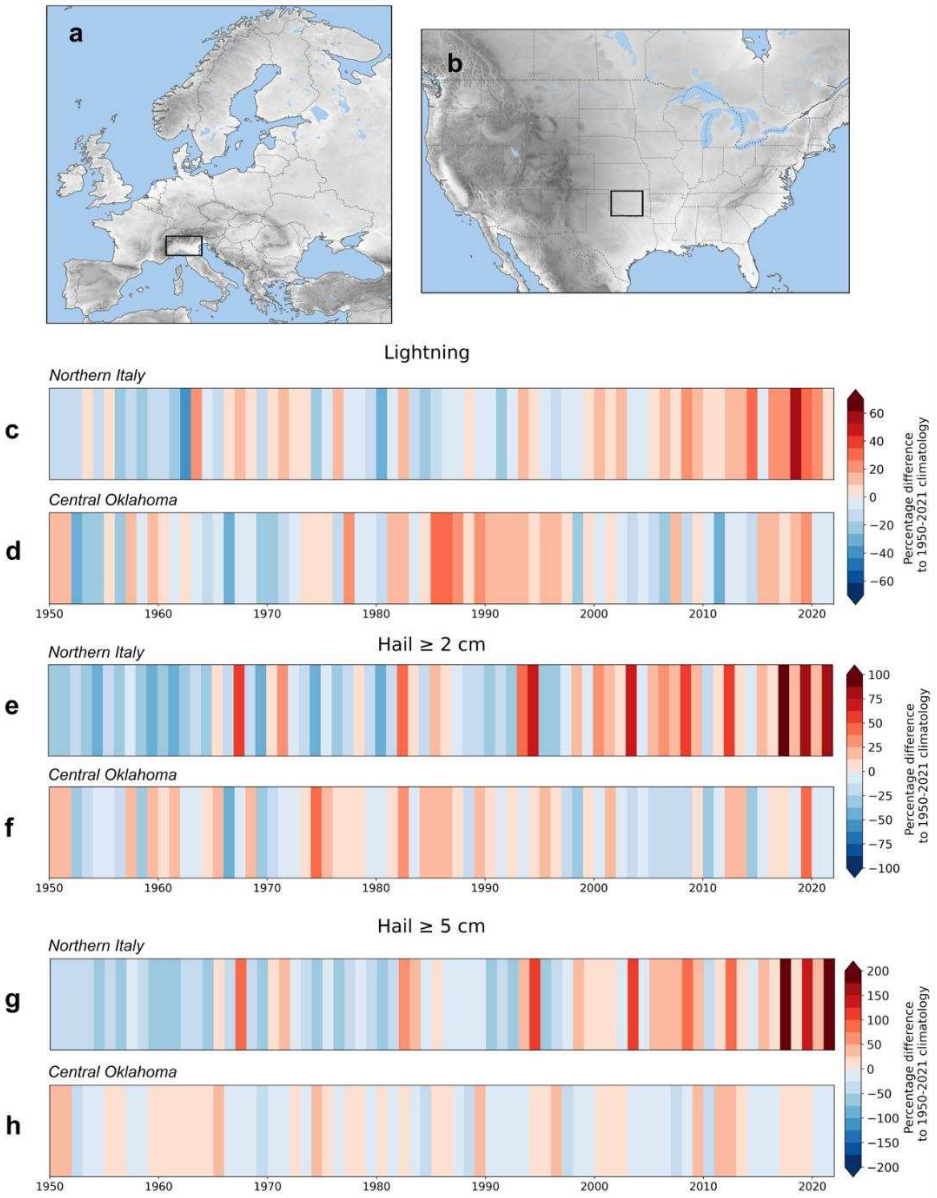

Preprints (www.preprints.org) | NOT PEER-REVIEWED | Posted: 3 August 2023 doi:10.20944/preprints202308.0314.v1

Figure 8. Modelled timeseries of lightning **(c,d)**, hail ≥ 2 cm **(e,f)**, hail ≥ 5 cm **(g,h)** across **(a)** northern Italy (44.5°N – 46.5°N , 7.25°E – 12.25°E) and **(b)** Central Oklahoma (34°N – 37°N, 260°E – 263.5°E) between 1950 and 2021. Colors indicate the area-averaged percentual departure of each hazard from the long-term (1950-2021) average.

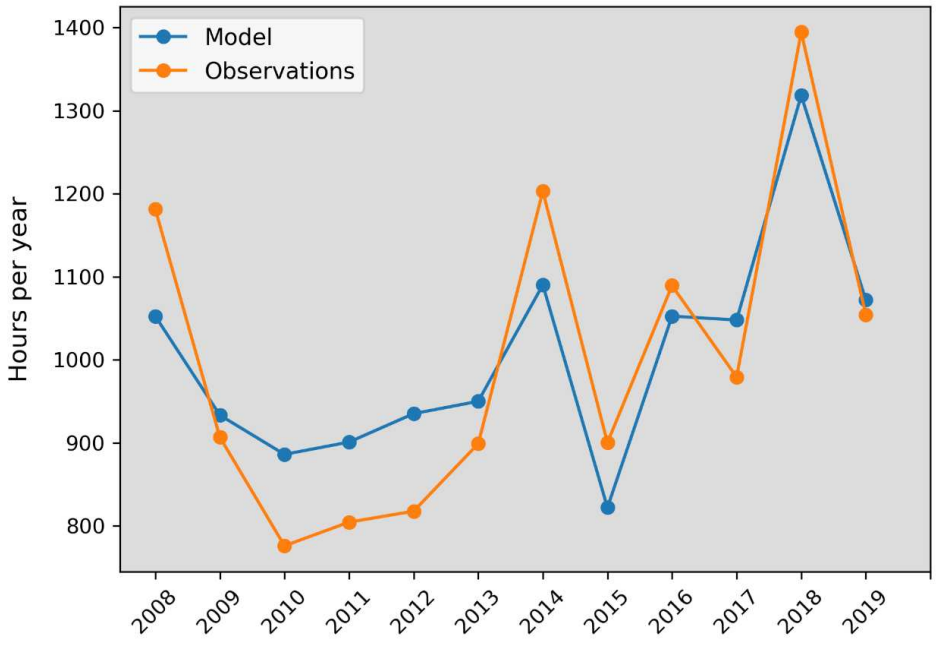

Figure 9. Comparison of modelled (blue) and observed (orange) sum of lightning hours per year across northern Italy (44.5°N – 46.5°N, 7.25°E – 12.25°E).

Although no significant trend was detected in Oklahoma between 1950 and 2021 (Figure 5), a period with above average activity occurred in the 1980s and the early 1990s, which explains differences in the detected trends between this study (no significant trend detected) and Taszarek et al. 2021a (negative significant trend across the southern Plains) where the trend was calculated since 1979. This is quantitively confirmed by the computed trend which exhibit opposite sign in the two periods: +1.1 hours per decade for 1950–2021 and -3.7 hours per decade for 1979–2021. The period of high activity corresponds well with enhanced signal from convective precipitation ($r = 0.88$, p-value: < 0.01) and mid-level relative humidity (Appendix C).

The 'hail stripes' display a stronger upward trend for hail compared to lightning across northern Italy. This upward trend is particularly steep for hail ≥ 5 cm, especially from 2010 onward when the rate of increase (0.09 annual hours per decade) more than quadrupled compared to the most recent climatological period (1992–2021) average trend (0.02). Across northern Italy, the three most active hail years have all occurred after 2016 and hail ≥ 5 cm is now 3 times more likely than what it used to be in the 1950s.

Inter-annual variability is much stronger for hail ≥ 5 cm (58.5% standard deviation between 1950 and 2021) and hail ≥ 2 cm (34.6 %) than for lightning (15.2 %). Together with an increase in frequency year-to-year variability in hail occurrence has increased with year-to-year variations exceeding 100% (hail ≥ 2 cm) and 200% (hail ≥ 5 cm) after 2016. Differently from northern Italy, no significant trend can be identified for Oklahoma.

We explored the relation between detected trends in lightning, hail ≥ 2 cm and hail ≥ 5 cm and two multi-decadal climate modes of variability, the Pacific Decadal Oscillation (PDO) and the Atlantic Multidecadal Oscillation (AMO). A significant correlation was found between lightning frequency in central Oklahoma and the seven-year running average PDO index ($r = 0.75$, p-value < 0.01). There is a good correspondence between the positive PDO phase and the above average lightning activity across the region during the 1980s and early 1990s (Figure 10). Hail ≥ 2 cm in Central

Preprints (www.preprints.org) | NOT PEER-REVIEWED | Posted: 3 August 2023 doi:10.20944/preprints202308.0314.v1

Oklahoma is also positively correlated with the PDO index (r = 0.60, p-value < 0.01) while a weak negative but insignificant correlation exists between hail ≥ 5 cm and the PDO index (r = -0.22, p-value = 0.08). Compared to Oklahoma, a weaker correlation was found between modelled trends and climate modes of variability in northern Italy e.g., the AMO (r = 0.39 for lightning, 0.35 for hail ≥ 2 cm, 0.40 for hail ≥ 5 cm all with a p-value < 0.01). Here, the sharp increase detected in modelled lightning, hail ≥ 2 cm and hail ≥ 5 cm over the last decade cannot be explained by a strengthening of the positive AMO phase, since this has remained approximately constant in the past two decades. The positive trend in these hazards is rather forced by local changes independent of the AMO, most importantly an increase in low-level moisture (MU_MIXR) and buoyancy in the form of the Most Unstable CAPE above the -10° C isotherm (Appendix C).

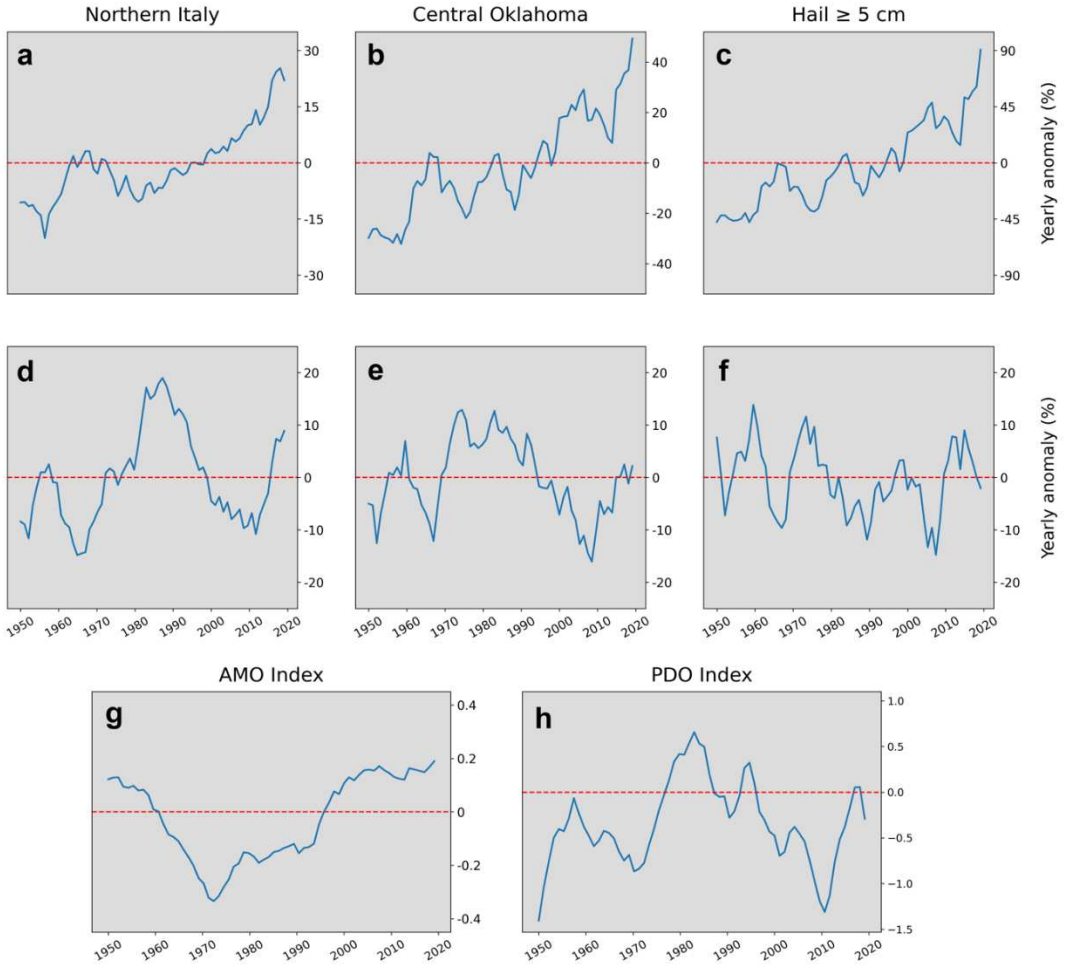

Figure 10. Seven year moving-average timeseries of modelled lightning **(a,d)**, hail ≥ 2 cm **(b,e)**, hail ≥ 5 cm occurrence **(c,f)**, AMO Index **(g)** and PDO Index **(h)**. Hazard time series are shown for **(a, b, c)** northern Italy (44.5°N – 46.5°N , 7.25°E – 12.25°E) and **(d, e, f)** Central Oklahoma (34°N – 37°N, 260°E – 263.5°E).

The annual cycles for three subperiods of equal length 1950–1973, 1974–1997 and 1998–2021 illustrate the seasonal changes during the 1950–2021 period (Figure 11). In each of these subperiods, lightning, hail ≥ 2 cm, and hail ≥ 5 cm have a sharp summer peak in North Italy, while lightning activity across Oklahoma reaches a plateau between May and August. In Oklahoma, the maxima in hail ≥ 2 cm and hail ≥ 5 cm do not directly correspond with that of lightning as it does in Italy: hail ≥ 2 cm and hail ≥ 5 cm are most common during late spring/beginning of summer before progressively decreasing, while lightning activity remains high through late summer.

Preprints (www.preprints.org) | NOT PEER-REVIEWED | Posted: 3 August 2023 doi:10.20944/preprints202308.0314.v1

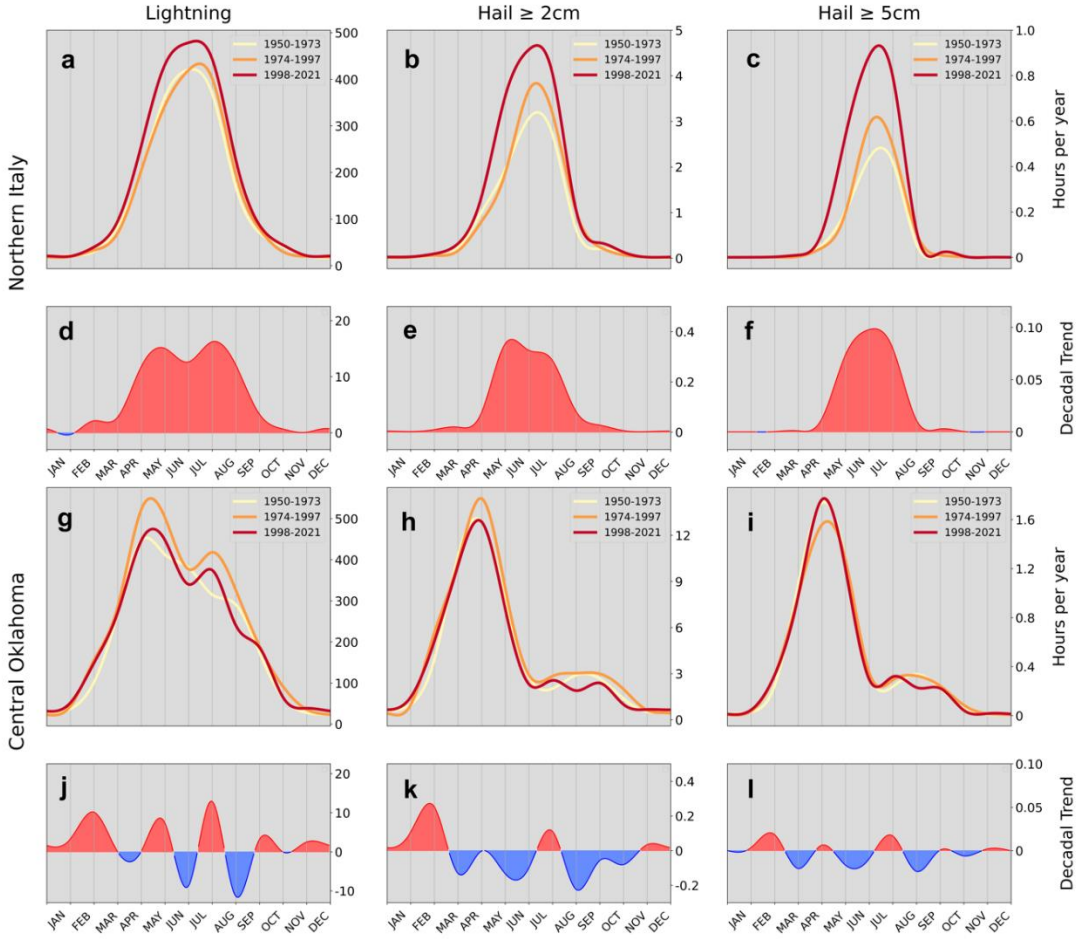

Figure 11. Modelled seasonal cycle of lightning **(a,g)**, hail ≥ 2 cm **(b,h)**, hail ≥ 5 cm **(c,i)** for three different periods (1950–1973, 1974–1997, 1998–2021 across northern Italy and Central Oklahoma. The mean trends for the three period are also shown for lightning **(d,j)**, hail ≥ 2 cm **(e,k)** and hail ≥ 5 cm **(f,l)**. Seasonal cycles were smoothed using a B-spline interpolation.

Since 1950, an increase in lightning, hail ≥ 2 cm and hail ≥ 5 cm occurs across northern Italy, especially comparing 1998–2021 to 1974–1997. The sharpest increase is observed for hail ≥ 5 cm. There is also a tendency for lightning and hail to start earlier in the year. May is the month with the strongest percentual increase in the period 1998–2021 (+90 % for hail ≥ 2 cm and +200 % for hail ≥ 5 cm compared to 1950–1997). In contrast to North Italy, the occurrence of lightning, hail ≥ 2 cm and hail ≥ 5 cm in Oklahoma does not see a monotonous increasing pattern. Lightning has become more common during winter, May, and July while its frequency has decreased in June and August. Most of these detected trends are influenced by the period of enhanced lightning activity between the 1980s and 1990s. Seasonal changes in hail ≥ 2 cm and hail ≥ 5 cm in central Oklahoma are small and non-significant.

7. Discussion and conclusion

We developed logistic models for lightning, hail ≥ 2 cm and hail ≥ 5 cm across Europe and the U.S. using hail reports, lightning observations, and atmospheric parameters from the ERA5 reanalysis. Reconstructions of the past (1950–2021) hail and lightning occurrence represent the observed patterns from storm reports, radar and satellite well across Europe (Punge et al. 2017, Taszarek et al. 2020a) and the U.S. (Cintineo et al. 2012; Bang and Cecil 2019; Wendt and Jirak 2021).

That being said, there are several limitations to the approach taken in this study. For example, the models have systematic biases in particular regions and months. For the lightning model, such

biases include an underestimation across Turkey, a slight overestimation across northern Europe as well as a general underestimation in summer. These biases may propagate to the modeled hail climatologies. Fundamental sources of error include the fact that the training datasets are limited to specific regions of good reporting rate, especially across Europe, and that the reanalysis contains errors as well. Such a reanalysis error is present across northern Europe, where ERA5 overestimates instability when compared to sounding observations (Pilguj et al. 2022) resulting in an overestimation of the lightning activity (Figure 3).

Another possible source of error is the omission of certain factors that influence the risk of lightning and hail, but which were not reflected by any of the candidate predictors. By taking an approach motivated by ingredients, i.e., known physical prerequisites for severe storms, we have tried to lower the risk of omitting crucial factors. A comparison of severe weather events that were poorly predicted with the models can be carried out to help reveal the missing factors and improve the models further. A particular difficulty is predicting the correct convective mode, since similar environments can produce very different storm types and associated convective hazards (Doswell and Evans 2003).

To trust the reconstructions of lightning and hail occurrence during the reanalysis era, it is necessary to have confidence that the models do not artificially introduce multi-year trends. Such trends may arise when areas in a parameter space with few observations in the training data set are poorly sampled by the model because they rarely occur in the training data set. For the reconstruction of the past climatology since 1950, we expect this to be a minor factor as the regions of parameter space visited in the 2020s differ only slightly from those visited in the 1950s. For applications of the models to extreme future climate projections, this may, however, be an issue to consider.

Regarding model errors, we want to point out that the reconstructions since 1979 do not fully agree with the studies by Tang et al. (2019) and Taszarek et al. (2021b), since they employ forecast parameters like SHP, LHP, or SCP, that do not take convective initiation into account. The most important resulting difference is over the Rocky Mountains and the southern High Plains into Mexico where AR-CHaMo models a decrease in thunderstorms since 1979. The error one would make when considering such parameters accurate proxies for hail would be large in those regions.

Much less difference in the nature and magnitude of the hail trends exists across one particular region: northern Italy. Here, according to AR-CHaMo, large increases in low-level moisture have already led to a very important increase in the occurrence of hail ≥ 5 cm by a factor of 3 since the 1950s.

Besides increasing probability, interannual variability in Europe has increased as well. An important open question is whether these sharp variations in hail activity can be explained in terms of the prevalence of certain atmospheric patterns and, if so, how the probability of large hail or convective initiation is related to the occurrence of specific atmospheric flows? Across the U.S., the underlying reasons behind the 1980s-1990s period of enhanced convective activity are still unknown and should be investigated further.

Apart from multi-year climate studies, the developed models also have potential application in forecasting, of which we do not yet present results here. Such efforts will require recalibration and renewed validation, since numerical weather prediction (NWP) models used in forecasting will have somewhat different climatologies of the predictor parameters than ERA5. The models may prove most useful in the medium-range, i.e., 2–10 days ahead, for which models that explicitly treat convection are not typically run. At such lead times, the use of ensemble forecasts rather than deterministic forecasts can add significant forecast skill. Another extension of the present work is to develop such models for other convective hazards, like tornadoes, severe convective wind gusts, intense convective rainfall and to extend the analysis to global scale.

Data Availability Statement: ATDnet and NLDN lightning observations were respectively provided by the UK Met Office and VAISALA. Both datasets cannot be provided due to the proprietary nature of the data. ESWD data are available from the ESSL and can be used under the terms of their respective User Agreement. For verifying this study, ESSL will provide the data for free. U.S. severe weather reports were provided by the SPC

 doi:10.20944/preprints202308.0314.v1

and are available at https://www.spc.noaa.gov/wcm/. ERA5 post-processed data was obtained from Dr. Mateusz Taszarek and can be made available. Contact mateusz.taszarek@amu.edu.pl for usage information.

Acknowledgments: This work was funded by the German Ministry of Education and Research for project 01LP1902G "CHECC", part of the Research Programme "ClimXtreme". Groenemeijer and Púčik's contributions were funded by the Austrian Science Fund (FWF) project P33113-N "PreCAST". Taszarek's contribution was funded by the Polish National Science Centre grant (project 2020/39/D/ST10/00768). The reanalysis computations were performed at the Poznan Supercomputing and Networking Center (project 448). We would like to thank and acknowledge ECMWF and the Copernicus Programme for the ERA5 reanalysis data, VAISALA and the Met Office for their respective ATDnet and NLDN lightning detection data, NOAA/SPC for Storm Data, the many volunteers and ESSL staff for their reports to the ESWD.

Appendix A – List of predictors for lightning, hail ≥ 2 cm and hail ≥ 5 cm model selection

Table A1. Atmospheric parameters tested as predictors for the lightning model. Parameters are listed into three categories: instability, mid-level humidity and other parameters relevant for convective initiation.

Instability	Mid-Level Humidity	Other
Mixed Layer CAPE	Mean Relative Humidity 500-850 hPa	Convective precipitation
Most Unstable CAPE	Mean Relative Humidity 700-850 hPa	Total precipitation
Surface Based CAPE	Mean Relative Humidity 500-700 hPa	Equilibrium Level
Hail Growth Zone CAPE	Mean Relative Hail Growth Zone	Land Sea Mask
Most Unstable CAPE above -10°C	Mean Relative Humidity 2-5 km	Convective Inhibition
Most Unstable CAPE above 500 m	Mean Relative Humidity 3-6 km	Mixing Ratio
Most Unstable (500 m) CAPE above -10°C		Vertical velocity at 3 km
Most Unstable Lifted Index		Vertical velocity at 5 km
3-6 km Lapse Rates		Moisture flux 0-2 km
2-4 km Lapse Rates		Convergence at 925 hPa

 doi:10.20944/preprints202308.0314.v1

Table A2. Atmospheric parameters tested as predictors for the hail ≥ 2 cm and hail ≥ 5 cm models. Parameters are organized into three categories: instability, wind shear and other parameters relevant for hail formation/growth.

Instability	Wind Shear	Other
Mixed Layer CAPE	0-6 km Bulk Shear	Lifting Condensation Level
Most Unstable CAPE	0-8 km Bulk Shear	Level of Free Convection
Surface Based CAPE	1-6 km Bulk Shear	Height of the 0° isotherm
Hail Growth Zone CAPE	Hail Growth Zone Bulk Shear	Wet Bulb 0° height
Most Unstable CAPE above -10°C	Bulk Shear surface to -10°	0-3 km Storm Relative Helicity
Most Unstable CAPE above 500 m	Bulk Shear surface to -20°	Warm Cloud Depth
Most Unstable (500 m) CAPE above -10°C	Bulk Shear 1 km to -10°	Precipitable Water
Most Unstable Lifted Index	Effective Mixed Layer Bulk Shear	Mixed Layer Mixing Ratio
3-6 km Lapse Rates	Effective Most Unstable Bulk Shear	Equilibrium Level
2-4 km Lapse Rates	Effective Surface Based Bulk Shear	Relative Humidity 0-2 km

Preprints (www.preprints.org) | NOT PEER-REVIEWED | Posted: 3 August 2023 doi:10.20944/preprints202308.0314.v1

Appendix B - Annual and seasonal mean and trend maps between 1979 and 2021

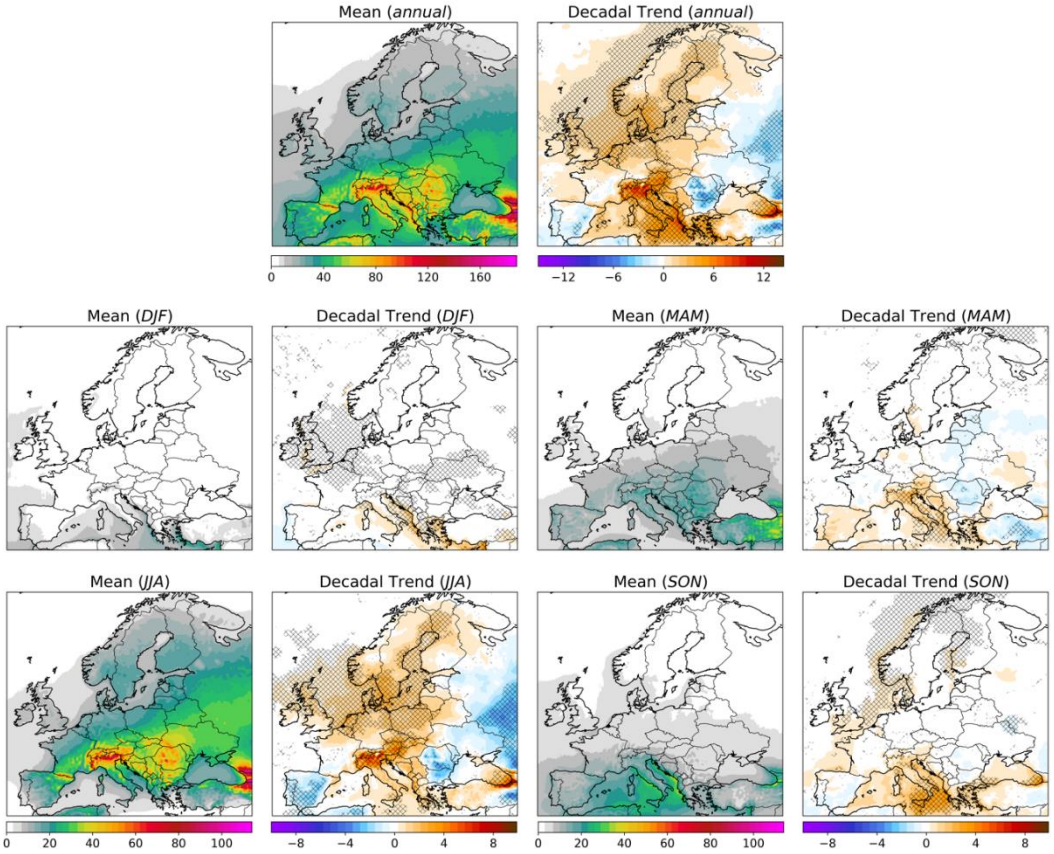

Figure A1. Mean modelled annual and seasonal number of lightning hours between 1979 and 2021 across Europe. Annual and seasonal trends are also shown and expressed as the change in the number of lightning hours per decade. Trends significant at a 95th percentile level are hatched.

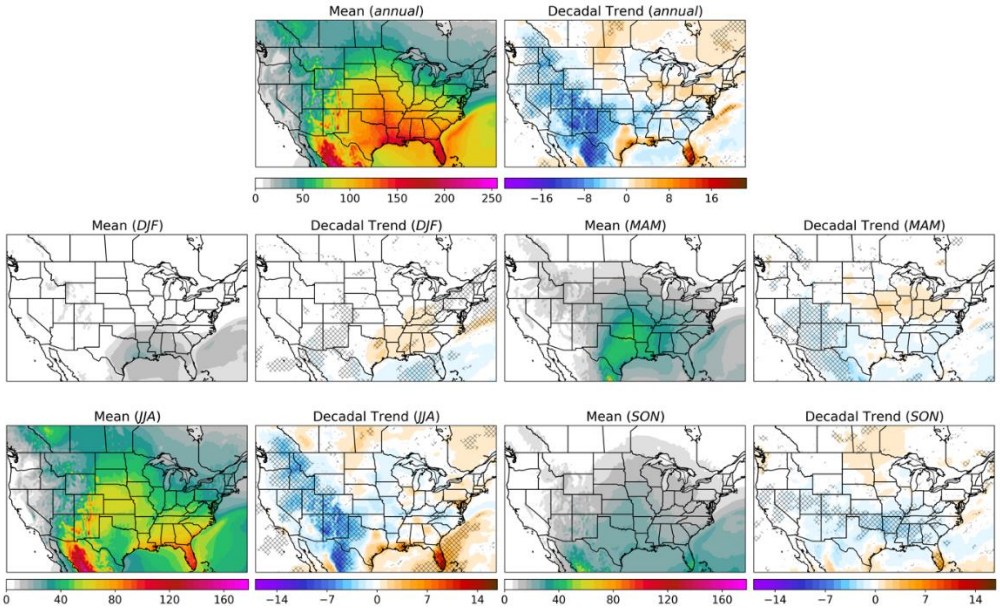

Figure A2. As for Figure A1, but for the U.S.

Preprints (www.preprints.org) | NOT PEER-REVIEWED | Posted: 3 August 2023 doi:10.20944/preprints202308.0314.v1

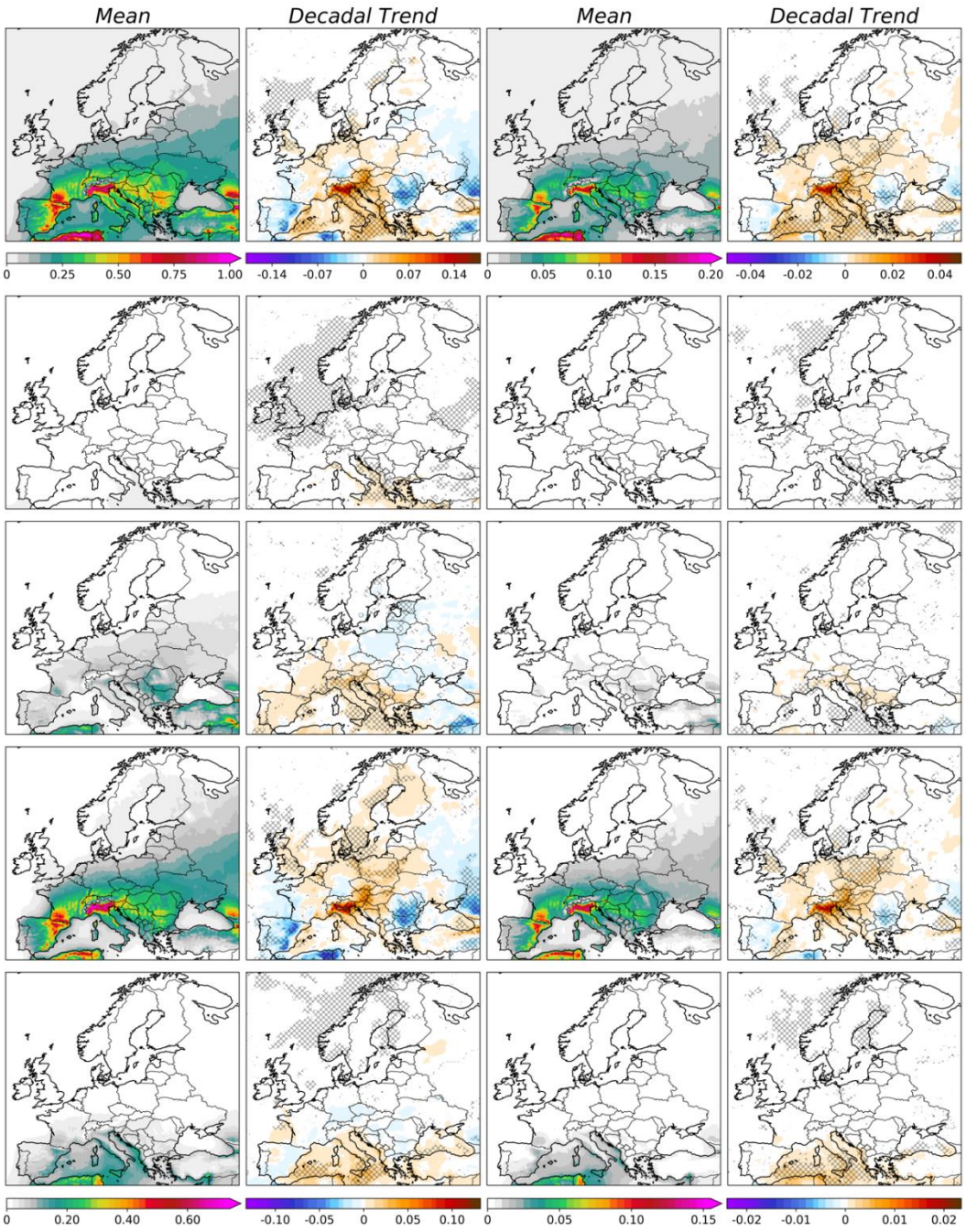

Figure A3. Mean modelled annual and seasonal number of hail hours (hail ≥ 2 cm and hail ≥ 5 cm) between 1979 and 2021 across Europe. Annual and seasonal trends are also shown and expressed as the change in the number of hail hours per decade. Trends significant at a 95th percentile level are hatched.

 doi:10.20944/preprints202308.0314.v1

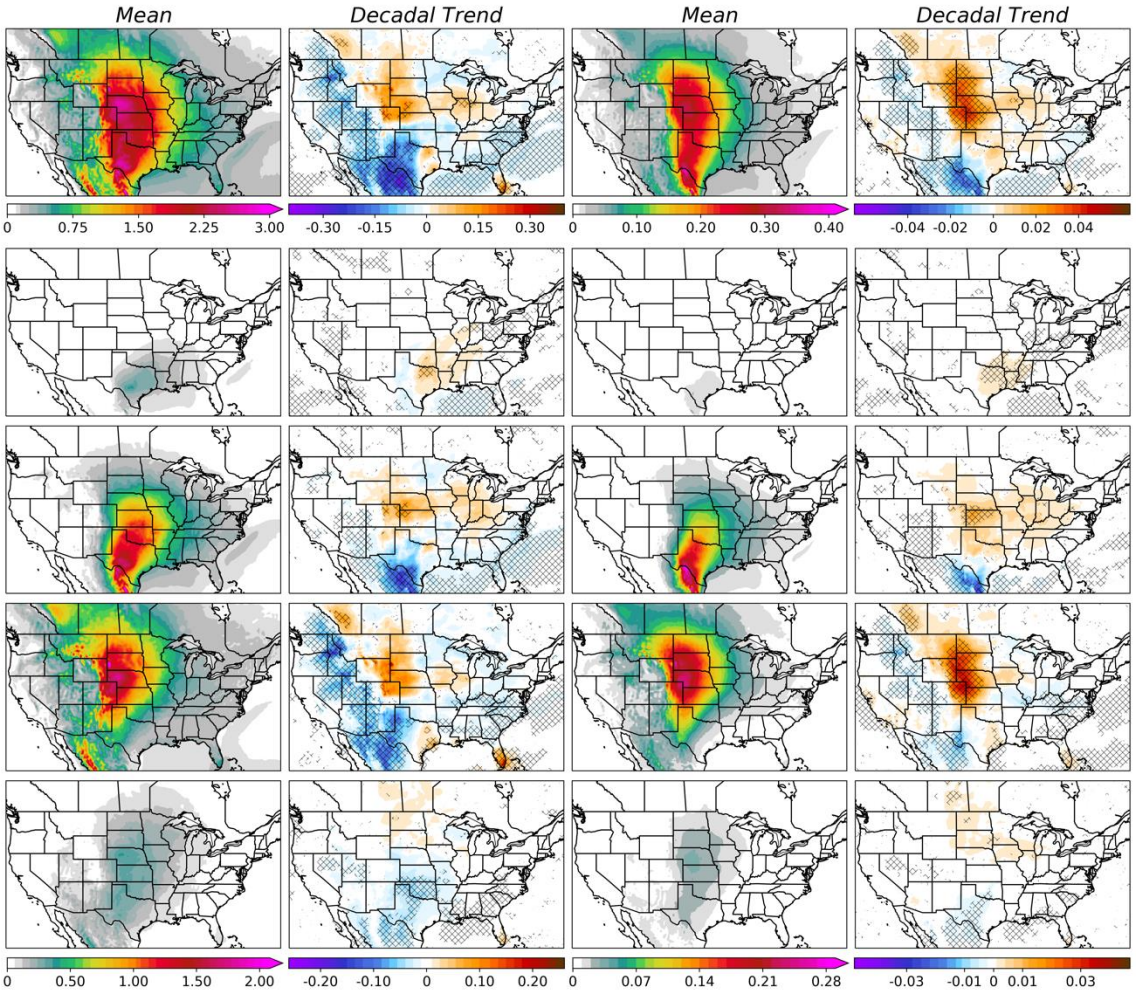

Figure A4. As for Figure A3, but for the U.S.

Preprints (www.preprints.org) | NOT PEER-REVIEWED | Posted: 3 August 2023 doi:10.20944/preprints202308.0314.v1

Appendix C – Additional stripes for hail and lightning model predictors

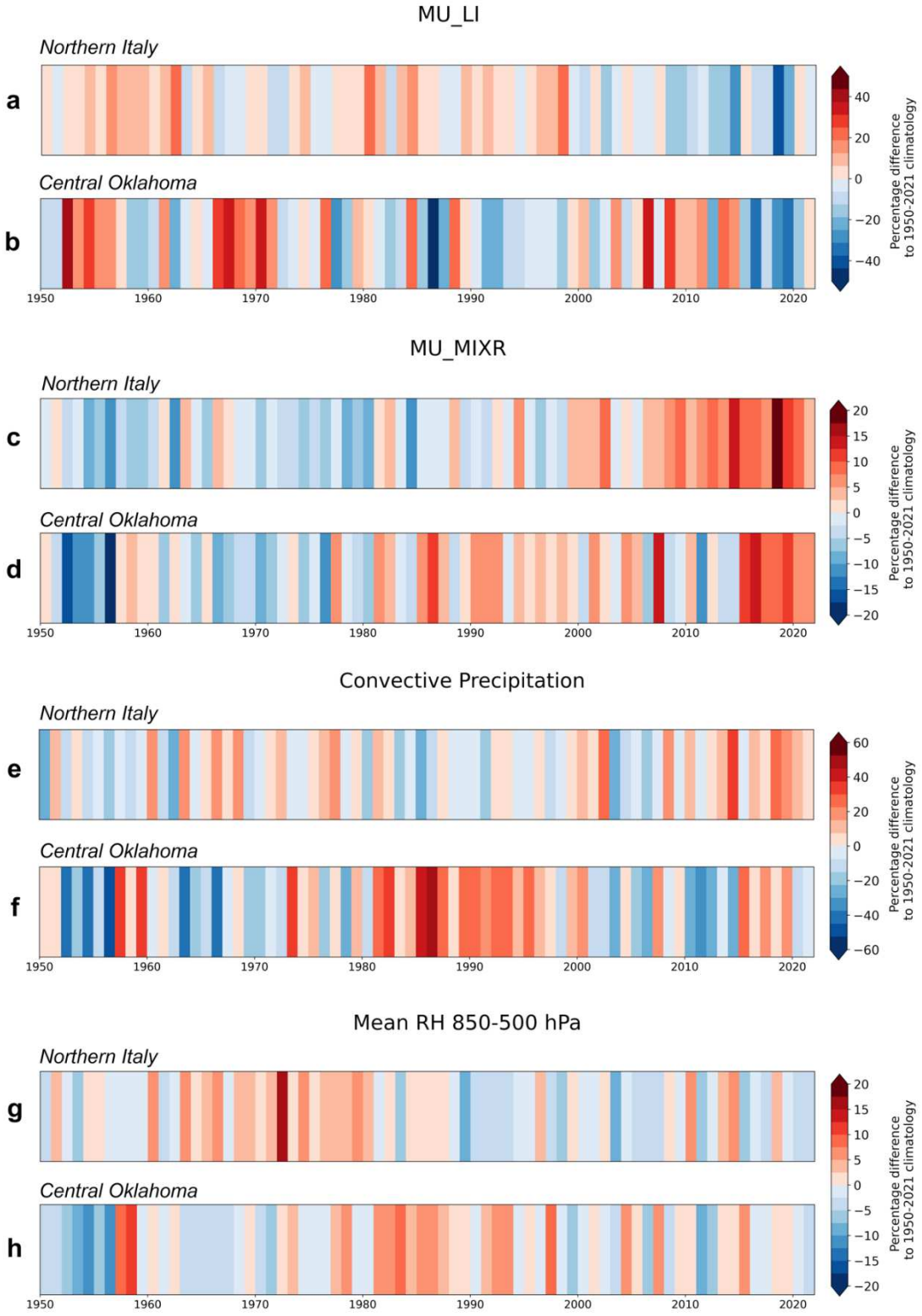

Figure A5. Modelled timeseries of lightning model predictors: most unstable lifted index **(a,b)**, most unstable mixing ratio **(c,d)**, convective precipitation **(e,f)**, mean relative humidity between 850 and 500 hPa **(g,h)** between 1950 and 2021 respectively across northern Italy and Oklahoma. Colors indicate the percentual departure from the long-term (1950-2021) average.

Preprints (www.preprints.org) | NOT PEER-REVIEWED | Posted: 3 August 2023 doi:10.20944/preprints202308.0314.v1

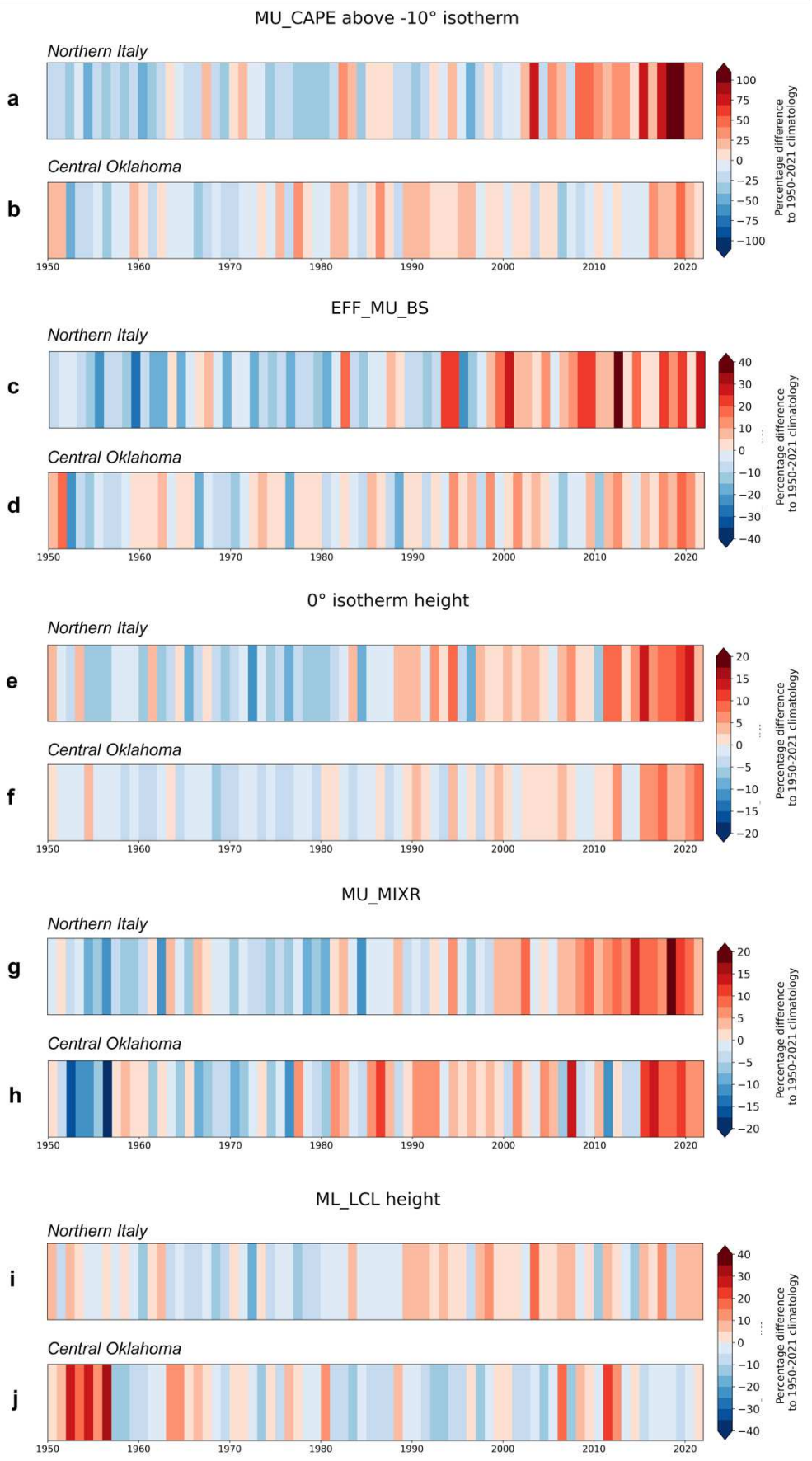

Figure A6. As for Figure A5, but for the hail ≥ 2 cm and hail ≥ 5 cm predictors: most unstable 500 m CAPE above the -10°C isotherm **(a,b)**, effective most unstable bulk shear **(c,d)**, height of the 0° isotherm **(e,f)**, most unstable mixing ratio **(g,h)**, lifting condensation level **(i,j)**.

References

1. Allen, J., and M. Tippett, 2015: The Characteristics of United States Hail Reports: 1955-2014. *E-Journal of Severe Storms Meteorology*, **10**, 1-31, doi:10.55599/ejssm.v10i3.60.
2. Allen, J. T., M. Tippett, and A. Sobel, 2015: An empirical model relating United States monthly hail occurrence to large-scale meteorological environment. *J. Adv. Model. Earth Syst.*, **7**, 226–243, https://doi.org/10.1002/2014MS000397.
3. Allen, J., I. Giammanco, M. Kumjian, H. Jurgen Punge, Q. Zhang, P. Groenemeijer, M. Kunz, and K. Ortega, 2020: Understanding Hail in the Earth System. *Reviews of Geophysics*, 58, doi:10.1029/2019rg000665.
4. Anderson, G. and Klugmann, D., 2014: A European lightning density analysis using 5 years of ATDnet data. *Nat. Hazards Earth Syst. Sci.*, **14**(4), 815-829, https://doi.org/10.5194/nhess-14-815-2014.
5. Bang, S., and D. Cecil, 2019: Constructing a Multifrequency Passive Microwave Hail Retrieval and Climatology in the GPM Domain. *J. Appl. Meteor. Climatol.*, **58**, 1889-1904, doi:10.1175/jamc-d-19-0042.1.
6. Bedka, K., Brunner, J., Dworak, R., Feltz, W., Otkin, J. and Greenwald, T., 2010: Objective Satellite-Based Detection of Overshooting Tops Using Infrared Window Channel Brightness Temperature Gradients. *J. Appl. Meteor. Climatol.*, **49**(2), 181-202.
7. Blair, S. and Coauthors 2017: High-Resolution Hail Observations: Implications for NWS Warning Operations. *Wea. Forecasting*, **32**, 1101-1119, doi:10.1175/waf-d-16-0203.1.
8. Brimelow, J., W. Burrows, and J. Hanesiak, 2017: The changing hail threat over North America in response to anthropogenic climate change. *Nature Climate Change*, **7**, 516-522, doi:10.1038/nclimate3321.
9. Cecil, D., and C. Blankenship, 2012: Toward a Global Climatology of Severe Hailstorms as Estimated by Satellite Passive Microwave Imagers. *J. Climate*, **25**, 687-703, doi:10.1175/jcli-d-11-00130.1.
10. Changnon, S. A., D. Chagnon, and S. D. Hilberg, 2009: Hailstorms across the nation: An atlas about hail and its damages. Contract Rep. 2009-12, 95 pp.
11. Cintineo, J., T. Smith, V. Lakshmanan, H. Brooks, and K. Ortega, 2012: An Objective High-Resolution Hail Climatology of the Contiguous United States. *Wea. Forecasting*, **27**, 1235-1248, doi:10.1175/waf-d-11-00151.1.
12. Craven, J. P., and H. E. Brooks, 2004: Baseline climatology of sounding derived parameters associated with deep, moist convection. *Natl. Wea. Dig.*, **28**, 13–24.
13. Czernecki, B., M. Taszarek, M. Marosz, M.Półrolniczak, L. Kolendowicz, A. Wyszogrodzki, and J. Szturc, 2019: Application of machine learning to large hail prediction—The importance of radar reflectivity, lightning occurrence and convective parameters derived from ERA5. *Atmos. Res.*, **227**, 249–262, https://doi.org/10.1016/j.atmosres.2019.05.
14. Dee, D., and Coauthors, 2011: The ERA-Interim reanalysis: Configuration and performance of the data assimilation system. *Quart. J. Roy. Meteor. Soc.*, **137**(656), 553–597, doi: 10.1002/qj.828.
15. Dennis, E. J., and M. R. Kumjian, 2017: The impact of vertical wind shear on hail growth in simulated supercells. *J. Atmos. Sci.*, **74**, 641–663, https://doi.org/10.1175/JAS-D-16-0066.1.
16. Dessens, J., C. Berthet, and J. Sanchez, 2015: Change in hailstone size distributions with an increase in the melting level height. *Atmos. Res.*, **158-159**, 245-253, doi:10.1016/j.atmosres.2014.07.004.
17. Doswell, C. A., Brooks, H. E., & Maddox, R. A., 1996: Flash flood forecasting: An ingredients-based methodology. *Wea. Forecasting*, **11**(4), 560-581.
18. Doswell, C. A., and J. S. Evans, 2003: Proximity sounding analysis for derechos and supercells: An assessment of similarities and differences. *Atmos. Res.*, **67–68 ,** 117–133.
19. Doswell, C., 2015: Severe convective storms in the European societal context. *Atmos. Res.*, **158-159**, 210-215, doi:10.1016/j.atmosres.2014.08.007.
20. Dotzek, N., P. Groenemeijer, B. Feuerstein, and A. M. Holzer, 2009: Overview of ESSL's severe convective storms research using the European Severe Weather Database ESWD. *Atmos. Res.*, **93**, 575–586, https://doi.org/10.1016/j.atmosres.2008.10.020.
21. Enno, S., Sugier, J., Alber, R. and Seltzer, M., 2020: Lightning flash density in Europe based on 10 years of ATDnet data. *Atmos. Res.*, **235**, 104769, https://doi.org/10.1016/j.atmosres.2019.104769.
22. Fluck, E., M. Kunz, P. Geissbuehler, and S. Ritz, 2021: Radar-based assessment of hail frequency in Europe. *Nat. Hazards Earth Syst. Sci.*, **21**, 683-701, doi:10.5194/nhess-21-683-2021.

23. Galway, J., 1956: The Lifted Index as a Predictor of Latent Instability. *Bull. Amer. Meteor. Soc.*, **37**, 528-529, doi:10.1175/1520-0477-37.10.528.
24. Gensini, V. A., Converse, C., Ashley, W. S., & Taszarek, M., 2021: Machine learning classification of significant tornadoes and hail in the U.S. using ERA5 proximity soundings. *Wea. Forecasting*, **36**(6), 2143–2160. https://doi.org/10.1175/WAF-D-21-0056.1
25. Groenemeijer, P., and A. van Delden, 2007: Sounding-derived parameters associated with large hail and tornadoes in the Netherlands. *Atmos. Res.*, **83**, 473-487, doi:10.1016/j.atmosres.2005.08.006.
26. Groenemeijer, P., and T. Kühne, 2014: A Climatology of Tornadoes in Europe: Results from the European Severe Weather Database. *Mon. Wea. Rev.*, **142**, 4775-4790, doi:10.1175/mwr-d-14-00107.1.
27. Groenemeijer, P., and Coauthors, 2017: Severe Convective Storms in Europe: Ten Years of Research and Education at the European Severe Storms Laboratory. *Bull. Amer. Meteor. Soc.*, **98**, 2641-2651, doi:10.1175/bams-d-16-0067.1.
28. Gunturi, P., and M. K. Tippett, 2017: Managing severe thunderstorm risk: Impact of ENSO on U.S. tornado and hail frequencies, WillisRe Technical Rep., 5 pp.
29. Hawkins, E. *Show Your Stripes.* 2018-2019. https://showyourstripes.info/.
30. Hersbach, H., and Coauthors, 2020: The ERA5 global reanalysis. *Quart. J. Roy. Meteor. Soc.*, **146**, 1999–2049, https://doi.org/10.1002/QJ.3802.
31. Johnson, A., and K. Sugden, 2014: Evaluation of Sounding-Derived Thermodynamic and Wind-Related Parameters Associated with Large Hail Events. *E-Journal of Severe Storms Meteorology*, **9**, 1-42, doi:10.55599/ejssm.v9i5.57.
32. Junghänel, T., Brendel, C., Winterrath, T. and Walter, A., 2016: Towards a radar- and observation-based hail climatology for Germany. *Meteor. Z.*, **25**(4), 435-445, doi:10.1127//metz/2016/0734.
33. Kirkpatrick, C., E. McCaul, and C. Cohen, 2009: Variability of Updraft and Downdraft Characteristics in a Large Parameter Space Study of Convective Storms. *Mon. Wea. Rev.*, **137**, 1550-1561, doi:10.1175/2008mwr2703.1.
34. Knaff, J., C. Sampson, and K. Musgrave, 2018: An Operational Rapid Intensification Prediction Aid for the Western North Pacific. *Wea. Forecasting*, **33**, 799-811, doi:10.1175/waf-d-18-0012.1.
35. Knight, C., and N. Knight, 2005: Very Large Hailstones From Aurora, Nebraska. *Bull. Amer. Meteor. Soc*, **86**, 1773-1782, doi:10.1175/bams-86-12-1773.
36. Koehlr, T., 2020: Cloud-to-Ground Lightning Flash Density and Thunderstorm Day Distributions over the Contiguous United States Derived from NLDN Measurements: 1993–2018. *Mon. Wea. Rev.*, **148**(1), 313-332, https://doi.org/10.1175/MWR-D-19-0211.1.
37. Kumjian, M., Z. Lebo, and A. Ward, 2019: Storms Producing Large Accumulations of Small Hail. *J. Appl. Meteor. Climatol.*, **58**, 341-364, doi:10.1175/jamc-d-18-0073.1.
38. Kumjian, M. R., and K. Lombardo, 2020: A hail growth trajectory model for exploring the environmental controls on hail size: Model physics and idealized tests. *J. Atmos. Sci.*, **77**, 2765–2791, https://doi.org/10.1175/JAS-D-20-0016.1.
39. Kumjian, M. R., and Coauthors, 2020: Gargantuan hail in Argentina. *Bull. Amer. Meteor. Soc.*, **101**, 1241-1258, doi:10.1175/bams-d-19-0012.1.
40. Kumjian, M., K. Lombardo, and S. Loeffler, 2021: The Evolution of Hail Production in Simulated Supercell Storms. *J. Atmos. Sci.*, **78**, 3417-3440, doi:10.1175/jas-d-21-0034.1.
41. Kunz, M., Blahak, U., Handwerker, J., Schmidberger, M., Punge, H. J., Mohr, S., Fluck, E., and Bedka, K. M., 2017: The severe hailstorm in southwest Germany on 28 July 2013: Characteristics, impacts and meteorological conditions, *Quart. J. Roy. Meteor. Soc*, **144**, 231–250, doi:10.1002/qj.3197.
42. Lin, Y., and M. R. Kumjian, 2022: Influences of CAPE on Hail Production in Simulated Supercell Storms. *J. Atmos. Sci.*, **79**, 179-204, doi:10.1175/jas-d-21-0054.1.
43. Mahoney, K., M. A. Alexander, G.Thompson, J. J. Barsugli, and J. D. Scott, 2012: Changes in hail and flood risk in high-resolution simulations over Colorado's mountains. *Nat. Climate Change*, **2**, 125–131, doi:10.1038/nclimate1344.
44. McCaul, E. W., and M. L. Weisman, 2001: The sensitivity of simulated supercell structure and intensity to variations in the shapes of environmental buoyancy and shear profiles. *Mon. Wea. Rev.*, ***129***, 664–687. doi:10.1175/1520-0493(2001)129<0664:tsosss>2.0.co;2

45. Merino, A., Wu, X., Gascón, E., Berthet, C., García-Ortega, E. and Dessens, J., 2014: Hailstorms in southwestern France: Incidence and atmospheric characterization. *Atmos. Res.*, **140-141**, 61-75, https://doi.org/10.1016/j.atmosres.2014.01.015.
46. Mulholland, J., J. Peters, and H. Morrison, 2021: How Does LCL Height Influence Deep Convective Updraft Width?. *Geophys. Res. Lett.*, **48**, doi:10.1029/2021gl093316.
47. Murillo, E., C. Homeyer, and J. Allen, 2021: A 23-Year Severe Hail Climatology Using GridRad MESH Observations. *Mon. Wea. Rev.*, **149**, 945-958, doi:10.1175/mwr-d-20-0178.1.
48. Nisi, L., Martius, O., Hering, A., Kunz, M., and U. Germann, 2016: Spatial and temporal distribution of hailstorms in the Alpine region: A long-term, high resolution, radar-based analysis. *Quart. J. Roy. Meteor. Soc*, **142**, 1590–1604, doi:10.1002/qj.2771.
49. Nisi, L., A. Hering, U. Germann, and O. Martius, 2018: A 15-year hail streak climatology for the Alpine region. *Quart. J. Roy. Meteor. Soc.*, **144**, 1429-1449, doi:10.1002/qj.3286.
50. Pilguj, N., Taszarek, M., Kryza, M. and Brooks, H., 2022: Reconstruction of Violent Tornado Environments in Europe: High-Resolution Dynamical Downscaling of ERA5. *Geophys. Res. Lett.*, **49**(11), https://doi.org/10.1029/2022GL098242.
51. Podlaha, A., S. Bowen, and M. Lörinc, 2020: Weather, Climate & Catastrophe Insight: 2019 Annual Report. Annual Rep. AON, 83 pp., http://thoughtleadership.aon.com/Documents/20200122-if-natcat2020.pdf.
52. Poręba, S., Taszarek, M. and Ustrnul, Z., 2022: Diurnal and Seasonal Variability of ERA5 Convective Parameters in Relation to Lightning Flash Rates in Poland. *Wea. Forecasting*, **37**(8), 1447-1470, https://doi.org/10.1175/WAF-D-21-0099.1.
53. Prein, A. and Holland, G., 2018: Global estimates of damaging hail hazard. *Wea. and Climate Extremes*, **22**, 10-23, https://doi.org/10.1016/j.wace.2018.10.004.
54. Púčik, T., Groenemeijer, P., Rýva, D. and Kolář, M., 2015: Proximity Soundings of Severe and Nonsevere Thunderstorms in Central Europe. *Mon. Wea. Rev.*, **143**(12), 4805-4821, https://doi.org/10.1175/MWR-D-15-0104.1.
55. Púčik, T. and Coauthors, 2017: Future Changes in European Severe Convection Environments in a Regional Climate Model Ensemble. *J. Climate*, **30**, 6771-6794, doi:10.1175/jcli-d-16-0777.1.
56. Púčik, T., C. Castellano, P. Groenemeijer, T. Kühne, A. Rädler, B. Antonescu, and E. Faust, 2019: Large Hail Incidence and Its Economic and Societal Impacts across Europe. *Mon. Wea. Rev.*, **147**, 3901-3916, doi:10.1175/mwr-d-19-0204.1.
57. Punge, H., K. Bedka, M. Kunz, and A. Werner, 2014: A new physically based stochastic event catalog for hail in Europe. *Natural Hazards*, **73**, 1625-1645, doi:10.1007/s11069-014-1161-0.
58. Punge, H., Bedka, K., Kunz, M. and Reinbold, A., 2017: Hail frequency estimation across Europe based on a combination of overshooting top detections and the ERA-INTERIM reanalysis. *Atmos. Res.*, **198**, 34-43, https://doi.org/10.1016/j.atmosres.2017.07.025.
59. Rädler, A., Groenemeijer, P., Faust, E. and Sausen, R., 2019: Detecting Severe Weather Trends Using an Additive Regressive Convective Hazard Model (AR-CHaMo). *J. Appl. Meteor. Climatol.*, **57**(3), 569-587, https://doi.org/10.1175/JAMC-D-17-0132.1.
60. Rasmussen, R. M., and Heymsfield, A. J., 1987: Melting and Shedding of Graupel and Hail. Part II: Sensitivity Study, *J. Atmos. Sci.*, **44**(19), 2764-2782.
61. Romps, D., J. Seeley, D. Vollaro, and J. Molinari, 2014: Projected increase in lightning strikes in the United States due to global warming. *Science*, **346**, 851-854, doi:10.1126/science.1259100.
62. Romps, D., A. Charn, R. Holzworth, W. Lawrence, J. Molinari, and D. Vollaro, 2018: CAPE Times P Explains Lightning Over Land But Not the Land-Ocean Contrast. *Geophys. Res. Lett.*, **45**, 12,623-12,630, doi:10.1029/2018gl080267.
63. Schaefer, J.T., and R. Edwards, 1999: The SPC Tornado/Severe Thunderstorm Database, Preprints, 11th Conference on Applied Climatology, Dallas, TX, Amer. Meteor. Soc., 215 – 220.
64. Schaefer, J. T., Levit J. J., Weiss S. J., and McCarthy D. W., 2004: The frequency of large hail over the contiguous United States. Preprints, *14th Conf. on Applied Meteorology*, Seattle, WA, Amer. Meteor. Soc., 3.3. [Available online at http://ams.confex.com/ams/pdfpapers/69834.pdf.]
65. Schroeer, K., Trefalt, S., Schwierz, C., Hering. A., Germann, Urs. and Nisi, L., 2019: A Hail Storm., 10th European Conference on Severe Storms (ECSS), Kraków, POLAND, Severe Storms Laboratory, 111, https://meetingorganizer.copernicus.org/ECSS2019/ECSS2019-111.pdf.

66. Schwarz, G., 1978: Estimating the Dimension of a Model. *The Annals of Statistics*, **6**(2):461–464, DOI: 10.1214/aos/1176344136.
67. Storer, R., and S. van den Heever, 2014: Microphysical Processes Evident in Aerosol Forcing of Tropical Deep Convective Clouds. *J. Atmos. Sci.*, **70**, 430-446, doi:10.1175/jas-d-12-076.1.
68. Tang, B., Gensini, V. and Homeyer, C., 2019: Trends in United States large hail environments and observations. *npj Climate and Atmos. Sci.*, **2**(1), 45. https://doi.org/10.1038/s41612-019-0103-7.
69. Taszarek, M., J. Allen, P. Groenemeijer, R. Edwards, H. Brooks, V. Chmielewski, and S. Enno, 2020(a): Severe Convective Storms across Europe and the United States. Part I: Climatology of Lightning, Large Hail, Severe Wind, and Tornadoes. *J. Climate*, **33**, 10239-10261, doi:10.1175/jcli-d-20-0345.1.
70. Taszarek, M., Allen, J., Púčik, T., Hoogewind, K. and Brooks, H., 2020b: Severe Convective Storms across Europe and the United States. Part II: ERA5 Environments Associated with Lightning, Large Hail, Severe Wind, and Tornadoes. *J. Climate*, **33**(23), 10263-10286, https://doi.org/10.1175/JCLI-D-20-0346.1.
71. Taszarek, M., J. Allen, H. Brooks, N. Pilguj, and B. Czernecki, 2021a: Differing Trends in United States and European Severe Thunderstorm Environments in a Warming Climate. *Bull. Amer. Meteor. Soc.*, **102**, 296-322, doi:10.1175/bams-d-20-0004.1.
72. Taszarek, M., N. Pilguj, J. Allen, V. Gensini, H. Brooks, and P. Szuster, 2021b: Comparison of convective parameters derived from ERA5 and MERRA2 with rawinsonde data over Europe and North America. *J. Climate*, 1-55, doi:10.1175/jcli-d-20-0484.1.
73. Thompson, R. L., C. M. Mead, and R. Edwards, 2007: Effective storm-relative helicity and bulk shear in supercell thunderstorm environments. *Wea. Forecasting*, **22**, 102–115, https://doi.org/10.1175/WAF969.1.
74. Thompson, R. L., B. T. Smith, J. S. Grams, A. R. Dean, and C. Broyles, 2012: Convective modes for significant severe thunderstorms in the contiguous United States. Part II: Supercell and QLCS tornado environments. *Wea. Forecasting*, **27**, 1136–1154, https://doi.org/10.1175/WAF-D-11-00116.1.
75. Tippett M., Sobel A., Camargo S., Allen J., 2012: An empirical relation between U.S. tornado activity and monthly environmental parameters. *J. Climate*, **27**, 2983–2999. doi:10.1175/JCLI-D-13-00345.1.
76. Tippett, M., Lepore, C., Koshak, W., Chronis, T. and Vant-Hull, B., 2019: Performance of a simple reanalysis proxy for U.S. cloud-to-ground lightning. *Int. J. Climatol.*, **39**(10), 3932-3946, https://doi.org/10.1002/joc.6049.
77. Trapp, R. J., N. S. Diffenbaugh, and A.Gluhovsky, 2009: Transient response of severe thunderstorm forcing to elevated greenhouse gas concentrations. *Geophys. Res. Lett.*, **36**, L01703, doi:10.1029/2008GL036203.
78. Vinet, F., 2001: Climatology of hail in France. *Atmos. Res.*, **56**(1-4), 309-323.
79. Wendt, N., and I. Jirak, 2021: An Hourly Climatology of Operational MRMS MESH-Diagnosed Severe and Significant Hail with Comparisons to Storm Data Hail Reports. *Wea. Forecasting*, **36**, 645-659, doi:10.1175/waf-d-20-0158.1.
80. Westermayer, A., Groenemeijer, P., Pistotnik, G., Sausen, R. and Faust, E., 2017: Identification of favorable environments for thunderstorms in reanalysis data. *Meteor. Z.*, **26**(1), 59-70, doi:10.1127/metz/2016/0754.
81. Williams, E., and S. Stanfill, 2002: The physical origin of the land–ocean contrast in lightning activity. *Comptes Rendus Physique*, **3**, 1277-1292, doi:10.1016/s1631-0705(02)01407-x.
82. Wilks, D. S., 2006: Statistical Methods in the Atmospheric Sciences. *In International Geophysics Series*. Acedemic Press, second edi edition, DOI: 10.1016/B978-0-12-385022-5.00020-8.
83. Witt, A., D. Burgess, A. Seimon, J. Allen, J. Snyder, and H. Bluestein, 2018: Rapid-Scan Radar Observations of an Oklahoma Tornadic Hailstorm Producing Giant Hail. *Wea. Forecasting*, **33**, 1263-1282, doi:10.1175/waf-d-18-0003.1.
84. Wood, S. N. (2006). Generalized additive models : an introduction with R. Texts in statistical science, pages xvii, 392 p., DOI: 10.1111/j.1541-0420.2007.00905 3.x.
85. Zhou, Z., Q. Zhang, J. Allen, X. Ni, and C. Ng, 2021: How Many Types of Severe Hailstorm Environments Are There Globally?. *Geophys. Res. Lett.*, **48**, doi:10.1029/2021gl09.